CHALMERS
UNIVERSITY OF TECHNOLOGY

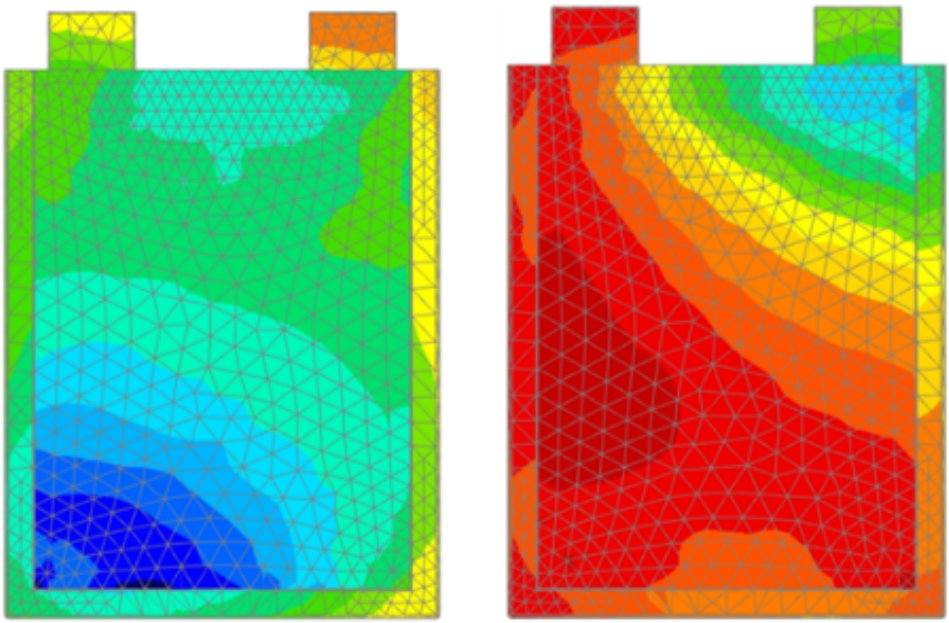

Loss verification of Li-Ion battery cell from thermal flow measurements

Master's thesis in Sustainable Energy Systems

ANDREW MANDEYA

DEPARTMENT OF ENERGY AND ENVIRONMENT

CHALMERS UNIVERSITY OF TECHNOLOGY
Gothenburg, Sweden 2023
www.chalmers.se

Master's thesis 2023

ANDREW MANDEYA

CHALMERS
UNIVERSITY OF TECHNOLOGY

Department of Energy and Environment
Division of Electric Power Engineering
Chalmers University of Technology
Gothenburg, Sweden 2023

Heat Generation Analysis of Lithium-Ion Pouch Cells using Calorimetric Methods
ANDREW MANDEYA

Supervisor: Istaq Ahmed, Volvo Group Trucks Technology
Examiner: Torbjörn Thiringer, Department of Energy and Environment

Master's Thesis 2023
Department of Some Subject or Technology
Division of Division name
Name of research group (if applicable)
Chalmers University of Technology
SE-412 96 Gothenburg
Telephone +46 31 772 1000

Gothenburg, Sweden 2023

ANDREW MANDEYA
Department of Energy and Environment
Chalmers University of Technology

Abstract

This master's thesis focuses on heat generation in Lithium-ion battery cells a crucial aspect affecting their performance, lifespan, and overall safety. A custom-made isothermal heat conduction calorimeter, integrated with heat flow sensors (Peltier elements), was used to measure heat flow from the lithium-ion cells. Initial experiments involved calibration and sensitivity testing using a 1.25 W resistor mat. Further heat generation experiments were conducted on lab-scale 0.25 mAh LiFePo4/Graphite cells and an 850 mAh lithium-polymer commercial pouch cell. These cells underwent electrochemical characterization tests, including formation cycles and electrochemical impedance spectroscopy (EIS), under various charge/discharge rates and temperatures. The calorimeter displayed reasonable sensitivity up to 6 mW, but higher noise levels were detected below this. Heat generation experiments were unsuccessful on the lab cells due to low dissipation of heat. However, measurements from the commercial cell agreed with established literature. The experimental results found that both irreversible (from internal cell impedance) and reversible (from electrochemical reactions) heat generation contribute to overall heat generation. Irreversible heat generation showed exothermic behaviour, especially during high current rates (especially in discharges direction), while reversible heat displayed both endothermic and exothermic behaviour and was more dominant at lower current rates (and is dependent on the state-of-charge). Interestingly, it was found that at low current rates endothermic behaviour was prominent for low state-of-charge levels while charging. Ambient temperatures significantly affected irreversible heat contributions due to resistance changes, but they did not notably impact reversible heat.

Keywords: Lithium-Ion, Battery, Pouch Cell, Heat Generation, Isothermal, Calorimetry, State-of-Charge, Electrochemical-Impedance-Spectroscopy

Acknowledgements

I would like to express my heartfelt gratitude to all those who have contributed to the completion of my master's thesis.

First and foremost, I am deeply thankful to my thesis advisor Istaq Ahmed for his unwavering support, and guidance throughout this research journey. I would also like to express my gratitude to Torbjörn Thiringer and Evelina Wikner for the insightful discussions and constructive feedback throughout the thesis journey. A special thanks to Fredrik Lindgren for his invaluable help during our study visit at Ångström Laboratory at Uppsala University.

I am also indebted to the colleagues at Volvo Group Trucks Technology for their insightful feedback and suggestions especially over fika discussions.

I extend my appreciation to my family and friends for their encouragement, and especially my lovely partner Tove for your unwavering support throughout the master's studies. Your emotional support provided the motivation to persevere through the challenges encountered during this academic pursuit.

Finally, I would like extend my gratitude to the Swedish Institute for Scholarships for providing me with the opportunity to pursue my master's education in Sweden.

Andrew Mandeya, Gothenburg, 2023

List of Acronyms

Below is the list of acronyms that have been used throughout this thesis listed in alphabetical order:

AC	Alternating Current
ARC	Accelerating Rate Calorimeter
BES	Battery Energy Storage
DC	Direct Current
HEV	Heavy Electric Vehicle
ICE	Internal Combustion Engine
LFP	Lithium Iron Phosphate
LMO	Lithium Manganese Oxide
LTO	Lithium Titanate
NMC	Lithium Nickel Cobalt Manganese Oxide
OCV	Open Circuit Voltage
SOC	State of Charge

Contents

1
Introduction

1.1 Background

In the 21st century, there is growing concern on the adverse effects of human activity onto the natural environment. The depletion of fossil fuels and consequent environmental pollution caused, are main contributors – therefore it is inevitable for modern society to reduce it's dependency on such fuel sources. The transportation sector is said to be responsible for up to 37 % of equivalent CO_2 emissions, where CO_2 a greenhouse-gas, is attributed to causing human induced climate change [3]. Hence, the use of Battery Electric Vehicles (BEVs) is increasing rapidly, where Li-Ion batteries (LIBs) are a crucial component of these vehicles. The adoption of BEVs is important from a climate change mitigation perspective, as they typically have a lower climate change impact compared to conventional fossil fuelled vehicles [10]. Therefore, it is important for automotive companies such as Volvo Group to understand the performance characteristics of LIB cells, such as the energy density and power capability qualities.

These characteristics have continuously improved over time, however it has come at the cost of safety and stability in the lithium-ion battery packs. With electric vehicles becoming more common, fire accidents caused by the lithium-ion batteries, are too occurring more frequently [18]. Therefore, it is of great importance for original equipment manufacturers (OEMs) such as Volvo Group to study the heat generation characteristics of lithium-ion batteries. Studying heat generation is invaluable for thermal modelling of LIB systems, where these models can allow engineers to predict the thermal behavior of LIB systems; establishing scenarios where these LIB systems exceed their safety limits. Furthermore, the results of these thermal models can inform engineers on designing effective thermal management systems, which ultimately will maximize the performance, safety and overall energy efficiency of these BEVs. This is an important step in supporting the transition to a more sustainable and low-carbon transportation system.

1.2 Purpose of work

The study of heat generation in lithium-ion cells is a complex task. There are several approaches that one can take such as through experimentation or computer simulation studies. The following thesis work will adopt an experimental approach where an existing battery lab environment at Volvo Group is used for the majority of the experimental work.

1.2.1 Scope

The scope of the thesis is therefore the following:

1. Study and improve the sensitivity to thermal flow of an existing isothermal-calorimeter setup

2. Assemble lab-scale pouch cells and perform heat generation and electrochemical tests using the calorimeter and battery testers

3. Compare heat generation and electrochemical characteristic tests to a commercial battery cell

4. Study the total heat generation rate (i.e., thermal power) and separate contributions of irreversible and reversible heat

1.2.2 Environmental and ethical considerations

As highlighted briefly in Section 1.1, the heat generation behaviour in lithium-ion batteries is a critical factor in advancing electric-vehicles (EVs) and ultimately reducing societies dependency on fossil fuels. As our dependence on electric-powered technologies, such as EVs and renewable energy storage systems, continues to increase, lithium-ion batteries and perhaps other energy storage technologies will become a crucial element in our technological infrastructure. However, the performance of these energy storage technologies are directly impacted by factors such as the heat generation rate, which typically manifest when losses and inefficiencies are present. By gaining a deeper understanding of such processes, researchers and engineers can work towards improving battery design to better manage heat and enhance overall performance. This can significantly enhance the safety of EVs and energy storage systems, fostering more widespread adoption of these sustainable technologies. Consequently, it would aid in reducing carbon emissions and our reliance on fossil fuels, thus contributing to global efforts against climate change - and making cleaner technologies more attractive to consumers. Therefore, studying and controlling heat generation in lithium ion energy storage technologies will play a critical role in societies transition to low carbon society.

In performing experimental work of this nature, it is vital for one to also consider the ethical perspective of such studies. The Institute of Electrical and Electronics

Engineers (IEEE) code of ethics provides a useful framework for which this thesis work is based on. An important aspect to consider is the overall health, safety and welfare of the general public when carrying out such studies [4]. For example, in an event that the results of this thesis work are used in real-world applications, it should not impose any risk on the health and safety of customers or the general public. Therefore, it is crucial that the reported results are accurate, honest and they are reported with great caution. The nature of experimental work is that there inevitable risks of error - therefore, it is crucial for the experiments to be repeatable in order to validate the accuracy of the results. Furthermore, in the event where there is unexpected results, they should still be presented, and not be hidden as to suit a desired conclusion or hypothesis. Finally, with the advent of globalization in the modern world, collaboration between different cultures and world-views is evermore important, this too has been considered through seeking input from individuals or other disciplines and worldviews.

2
Theory

The following chapter aims to provide theoretical background on the core aspects of the experimental work. At the heart of the thesis work is the lithium-ion battery cell - which is the primary test object during the experimental work. In addition, it is equally important to highlight the fundamental theory behind the experimental techniques used. Therefore, the following section will cover the working principle of LIB cells, calorimetry and the thermodynamics of heat generation.

2.1 Lithium-ion battery cells

A battery is defined as a chemical storage device and in the context of electric vehicles, a battery pack consists of a set of interconnected battery cells that power the electric motor and other electronic devices in the vehicle. The scope of the thesis is primarily on the individual battery cell level. Lithium-ion batteries (LIBs) have grown in popularity due to their high power density (W/kg) and energy density (Wh / kg) compared to other battery technologies such as Lead Acid batteries. A battery with high power and energy density is an important requirement for electric vehicles as it allows for more energy to be stored while reducing the size and weight of a battery pack - and ultimately, minimizing costs.

2.1.1 Working principle of a lithium-ion cell

The fundamental unit of a battery system is the battery cell also referred to as an electrochemical cell. A battery cell converts chemical energy to electric energy and vice-versa; where the process of converting chemical energy into electric energy is referred to as discharging, while the reverse process is referred to as charging. Battery cells that strictly undergo the discharging process are referred to as galvanic cells, while those that only undergo charging are referred to as electrolytic cells.

The fundamental design of an electrochemical cell consists of several key components namely: electrodes, separator, electrolyte and current collectors. The basic design is that lithium-ions move between positive (cathode) and negative (anode) electrodes through the electrolyte medium as illustrated in Figure 2.1. The positive and negative electrodes serve as the sites for which electrochemical reactions take place. These chemical reactions that occur during charge and discharge are based on electrochemical oxidation and reduction reaction processes, or simply redox reactions. During the redox reactions, electrons travel via an external circuit from one

electrode to another while aiming to maintain a balanced charge.

The oxidation reaction process takes place at the negative electrode (anode), where the electrons then travel via an external circuit (through the current collector) to the positive electrode (cathode), where now the electrons are accepted and the reduction processes occurs. Simultaneously, lithium-ions flow through the electrolyte and separator towards the cathode. This process is referred to as discharging, and vice-versa would be charging. Therefore, during discharging the anode is an electron donor, while the cathode is a electron acceptor.

During the operation of a LIB cell, the State of Charge (SOC) is an important measure of the battery cell's available energy. Essentially, the SOC refers to the amount of current energy capacity (in unit of Amp hours, Ah, or milli-Amp hours, mAh) of the battery as a percentage of its maximum energy capacity (Ah). For example, if a LIB cell has a maximum capacity of 100 mAh, and it's currently at 50 mAh remaining charge, then the SOC level would be 50 %. Typically, a LIB cell's upper and lower SOC limits are recommended by the manufacturer based on the tolerable voltage: 0 % SOC represents the lower voltage allowed (cut-off voltage), and 100 % representing the maximum voltage tolerable (voltage limit). These voltage limits are in place as to prevent under or over voltage scenarios that may lead to damages and worse-case, thermal runaway.

Accurately determining the SOC of a LIB cell is a challenging task as a LIB cell is dynamic in nature - often resulting in the true SOC level changing based on temperature, and more importantly, battery cell ageing - which is due to degradation overtime. The two main methods of estimating a LIB cell's SOC level is by coloumb counting, which is the integration of the amount of current (ampere) with time (hours). The other method is by open circuit voltage (OCV) relaxation, where the battery cell's SOC level is estimated by the open circuit voltage obtained after allowing a long relaxation period.

2.1.2 Cell Components

As highlighted in Section 2.1.1, a LIB cell consists of electrodes, separator, electrolyte, and current collectors. These components are classified into two main groups; active and non-active. The components where redox reactions take place are referred to as active components, while non-active components are those where there are no direct redox reactions. Therefore, generally speaking electrodes are active components - while everything else, such as the electrolyte, separator etc. are non-active components.

The electrode refers to an essential component within the battery cell where redox reactions occur during the charge and discharge processes. Typically, the active electrode is mixed with an electron-conducting and binder material to create a composite electrode [7]. The size, loading, surface area as well as the morphology of the particles in the active material affect the overall efficiency of the redox reactions;

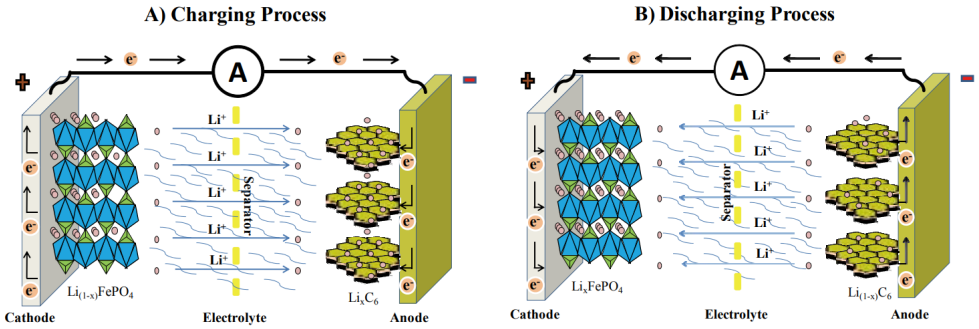

Figure 2.1: Schematic of the charging (A) and discharging (B) processes of a typical Li-ion cell [20].

thus the overall energy and power performance of a LIB cell. Lithium transition metal oxides such as lithium nickel cobalt aluminium oxide (NCA) are particularly popular as positive electrodes, as the lithium element is small in nature, and has a high energy density. While graphite, a natural occurring form of carbon, is popular in negative electrodes due to their sheer abundance and relative high energy density. In addition to its high conductivity, graphite serves as a hosting structure, where lithium ions are extracted from the positive electrode and stored in the graphite during the intercalation process. These materials are favourable for electron and ion flow allowing for redox reactions to occur spontaneously on the outermost surface layer of the material. Hence, the rise in popularity of LIB in electric vehicles, electronic devices and large-scale energy storage [7].

Separating the two electrodes is a separator which is typically a thin porous membrane that acts as a physical barrier to prevent the electrodes from directly contacting each other, while simultaneously allowing lithium ions to flow in between. Finally, another crucial element of the lithium ion battery is the electrolyte, which is a chemical solution that facilitates the flow of lithium ions between the two electrodes. The electrolyte is crucial as it provides a medium for the lithium ions to flow through and thus completing the circuit. The performance of a LIB cell is also influenced by the quality of the electrolyte. Electrolytes are typically a solution of one or several salts (e.g., $LiPF_6$) dissolved in organic solvents [15]. The electrolyte allows for Li-ion's to be conducted between the electrodes, and further insulates electron transport. Therefore, the main requirement of a electrolyte is for it's ion conductivity properties to be fast, as to allow for redox reactions to occur.

Finally, the current collectors are used at each electrode and they mainly serve the function of allowing for electrons to be transferred from one electrode to the other via an external circuit. Typically, thin foils of aluminium or copper are used as they have high conductive properties. Furthermore, the current collectors provide mechanical stability for the electrodes.

2.1.3 Cell Form Factor

LIB cells used in electric vehicles typically come in three designs: cylindrical, prismatic and pouch cells. Each of which have their own advantages and disadvantages.

Cylindrical

Cylindrical cells are the most recognizable shape of battery cells, and they are made from electrodes materials that are wound together in a "jelly-roll" shape as seen in Figure 2.2 b. These cells are often encapsulated in a hard casing as to provide mechanical strength. Their main advantage is they are typically faster and cheaper to manufacture compared to the other designs. However, a major challenge is they do not occupy space efficiently compared to a prismatic or pouch cell due to the nature of cylindrical geometry - hence they are not ideal when it comes to packaging.

Prismatic

Prismatic cells are rectangular shaped LIB cells that are typically enclosed in a metal casing as seen in Figure 2.2 a. The electrodes can either be wounded or stacked on top of each other. Like the cylindrical cell, the prismatic is encased with metal (typically aluminium metal casing) to improve the mechanical strength. The size of these cells tend to be larger than cylindrical and hence the overall capacity is usually higher. However, if packaging is not done carefully in a battery pack, then thermal management can be a challenge - where thermal propagation (spread of heat from cell to cell) becomes more likely.

Pouch

Finally, the pouch cell shares resemblance to the prismatic with the rectangular shape, however they are not enclosed in a metal casing, but instead in a pouch as seen in Figure 2.2 c. These pouches are normally made of a layer of aluminum-coated plastic film and thus allowing them to be light. Hence, pouch cells tend to be thinner allowing them to be packaged in a more efficient manner compared to prismatic and cylindrical. However, this comes at the cost of poor mechanical strength as their is no metal casing to protect the LIB cell. The electrodes are typically stacked or rolled in a Z-fold.

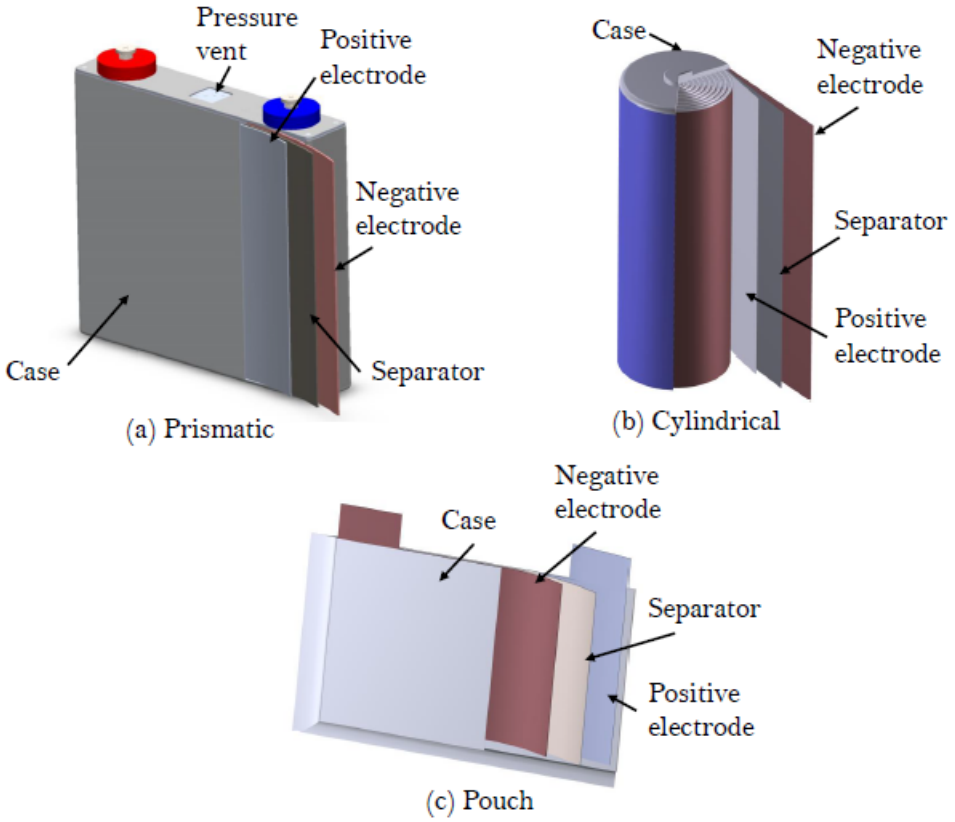

Figure 2.2: Popular LIB cell form factor designs [13].

2.2 Thermodynamics & Heat Generation

In understanding the heat generation and transfer processes that occur within LIB cells, it is important to discuss the underlying thermodynamic principles at play. Thermodynamics is a branch of physics that describes the relationships between heat, energy and work. In the context of LIB cells, these thermodynamic relationships help describe the underlying processes that cause heat generation within LIB cells.

Fundamentally, the potential difference between the electrodes of a LIB cell determines the theoretical *cell voltage* (E_{cell}) which is commonly referred to as the *electrochemical force* or *emf*. The emf of a cell can be expressed in terms of Gibbs free energy, ΔG_{cell}. The Gibbs free energy represents the theoretical maximum non-volume expansion work that can be achieved in a thermodynamically closed system at constant pressure and temperature. In a closed electrochemical system, the non-volume expansion work done is equivalent to the electrical energy output. Therefore, when the chemical energy in a LIB cell is converted into electrical energy under a reversible process, the electrical energy is equal to the Gibbs free energy. When the reaction occurs in the LIB cell, there is a decrease in the free energy of the cell according to [24]

$$\Delta G_{cell} = -nFE_{cell} \tag{2.1}$$

where:

G_{cell} : Gibbs free energy
n : Number of electrons involved in the reactions
F : Faraday constant (= 96485 As/mol)
E_{cell} : Cell electrochemical force (emf)

In addition, the Gibbs free energy is proportional to the change in entropy during the reaction according to [7]

$$\Delta G_{cell} = -nFE_{cell} = \Delta H - T\Delta S = \Delta H - nFT(\frac{\partial E_{cell}}{\partial T}) \tag{2.2}$$

The $\frac{\partial E_{cell}}{\partial T}$ term is referred to as the entropic heat coefficient, and is positive if heat is generated during charge. Conversely, heat will be consumed during discharge. The ΔS term represents the change in entropy, while ΔH represents the change in enthalpy.

The total ΔG_{cell} for any electrochemical cell can also be expressed as the difference between the sum of the free energy of both the products and the reactants according to

$$\Delta G_{cell} = \sum \Delta G_{prod} - \sum \Delta G_{react} \tag{2.3}$$

An electrochemical reaction is considered spontaneous (i.e. reaction does not require an external source) when $\Delta G_{cell} < 0$ (e.g. discharging). Conversely, if $\Delta G_{cell} > 0$, then the electrochemical reaction is non-spontaneous and requires an external source (e.g. charging).

In an ideal case, it is desirable to convert all Gibbs free energy into useful electrical energy during discharge. However energy losses caused by polarization is inevitable when a load current passes through the LIB cell. Polarization is a collective term used to describe (potentially unwanted) mechanical side-effects that influence reaction mechanisms and chemical kinetics. These polarization effects - analogous to electrical impedance - are the most influential factors that contributes towards energy losses in the LIB cell.

The total polarization of a LIB cell can be attributed to ohmic polarization, activation polarization and concentration polarization. Ohmic polarization is caused by the intrinsic electrical resistance to charge flow in the LIB cell resulting in voltage losses. This results in waste energy in the form of heat. The total ohmic polarization is the sum of the polarization caused by ionic resistances in the electrolyte, contact resistance in the active material and current collectors, and electrical resistances in the electrodes, current collectors and electrical tabs of both electrodes. The ohmic polarization is in agreement with Ohm's law (hence ohmic polarization) as it follows a linear relationship between the current and the voltage drop.

The activation polarization occurs in the beginning of life (BOL) of a LIB cell during the initial charge. The polarization results from the need to activate the electrochemical reactions at the electrode/electrolyte interface. On the other hand, the concentration polarization appears due to a concentration gradient between the active species (reactants and products) in the electrode/electrolyte interfaces. The concentration of the active species in the electrolyte decreases over time due to the formation of the SEI layer on the surface of the electrodes. Considering the above losses, the actual voltage (E_{cell}) of a LIB cell can be expressed according to:

$$E_{cell} = E_0 - [(\eta_{ct}) + (\eta_c)]_{pos} - [(\eta_{ct}) + (\eta_c)]_{neg} - iR_{cell} \tag{2.4}$$

where:

E_0 : Emf or open-circuit voltage of the cell
η_{ct}: Activation polarization at positive or negative electrode
η_c: Concentration polarization at positive or negative electrode
i: Operating current of cell on the load
R_i: Internal resistance of cell.

The total polarization occurring in the LIB cell result in the consumption of Gibbs energy, and ultimately waste heat energy being generated during the charge-discharge process. Furthermore, this inhibits the LIB cell from achieving the theoretical open-circuit voltage which can be seen visually in Figure 2.3.
Therefore, the general equation for heat generation in a Li-Ion cell is described by [22]:

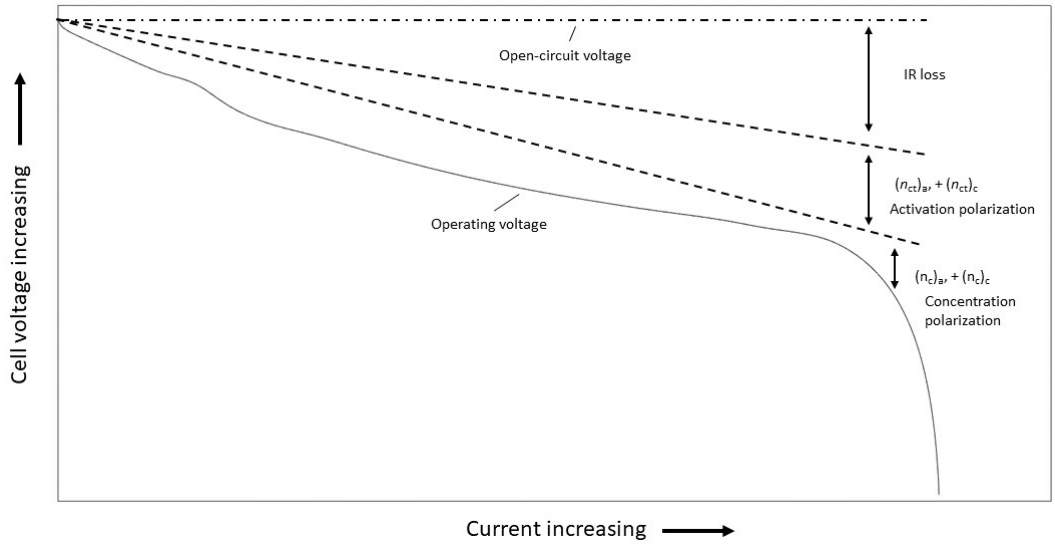

Figure 2.3: Cell polarization as a function of current. Adapted from [14].

$$Q_{bat} = Q_{generated} = Q_{irr} + Q_{rev} \tag{2.5}$$

$$Q_{bat} = Q_{generated} = I^2 R_{cell} + I T_{cell} \frac{\partial E_{OCV}}{\partial T_{cell}} \tag{2.6}$$

$$Q_{bat} = Q_{generated} = I(E - E_{OCV}) + I T_{cell} \frac{\partial E_{OCV}}{\partial T_{cell}} \tag{2.7}$$

where:

Q : Heat generated in battery cell
I : Is the current rate
E_{OCV} : Open circuit voltage
E : Output voltage of the cell
T_{cell} : Temperature of the cell
R_{int} : Internal Resistance of the cell

The heat generated in a Li-ion cell consists of both irreversible and reversible heat generation, where the former represents wasted heat energy due to the aforementioned polarization such as (Ohmic losses) and the latter representing entropic change (ΔS) due to the electrochemical reaction. The irreversible losses are exclusively exothermic, meaning that heat is released from the LIB cell, while reversible entropic heating can be either exothermic or endothermic as shown in Figure 2.4. The entropy change thermodynamic property which is responsible for the reversible heating during the intercalation and deintercalation of Li-ions during Redox, can be determined experimentally as discussed in Section 3.5.1.2.

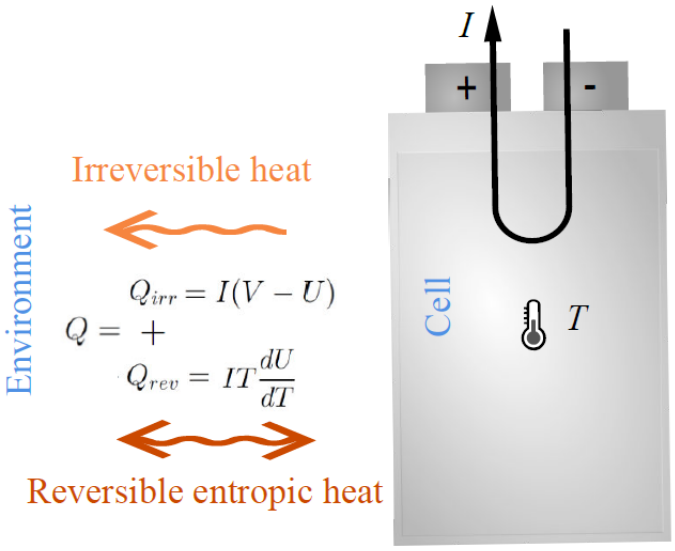

Figure 2.4: Heat generation in LIB cell [11].

2.3 Calorimetry

A calorimeter is an instrument used to measure the heat of chemical reaction or physical changes. The basic principle is that a calorimeter contains a vessel (or container) in which the sample being studied is placed. The surrounding area of the calorimeter is known as a shield, and there can be several shield layers to provide improved isolation of the sample.

Calorimeter instruments can be divided into the following main categories:

1. Adiabatic calorimetry in which there is no heat exchanged with the outside environment. In order to achieve this it is a prerequisite to have near perfect insulation so as to ensure that there no heat being added or removed from the system.

2. Non-adiabatic calorimetry are those that have exchange of between the vessel and the outside environment.

3. Isothermal calorimetry in which there is a constant shield temperature.

4. Non-isothermal calorimetry in which the shield temperature is not constant.

The calorimeter experimental setup used in the following thesis work is a isothermal conductive calorimetry.

2.3.1 Heat flow sensors (theromopiles)

The heat flow sensors that are integrated inside of the calorimeter are thermo-electric devices that are based on the Seebeck effect (the reverse being the Peltier effect) which is a phenomenon where a temperature difference will produce a voltage signal. The heat flow sensors consist of a large number of thermocouples connected in series electrically to produce a large voltage output, while also being connected in parallel thermally to produce a high voltage to temperature difference ratio. Typically, the thermocouples are made of p- and n-doped bismuth telluride [12]. The voltage difference ΔU is generated across the semiconductor material inside the heat flow sensors when a temperature difference ΔT is applied across the junctions of the material. The amount of voltage produced per temperature difference is referred to as the Seebeck coefficient - thus it defines the strength of the thermoelectric effect of the heat flow sensors. The Seebeck coefficient a (V/K) for a single thermocouple is defined by

$$\Delta U = a\Delta T \tag{2.8}$$

Within a heat flow sensor the Seebeck coefficient can be defined as $E = Na$, where N is the number of thermocouples in the thermoelectric device.
According to author Wadsö the sensitivity of a thermoelectric heat flow sensor is governed by the following properties [12]:

- The devices thermal conductance, K (W/K)
- The Seebeck coefficient, E (V/K)

These two coefficients relate both the heat flow rate through the heat flow sensors, as well as the voltage output for K and E respectively, to the difference between the sample and the heat sink in the calorimeter. Ultimately, the ratio between these two properties will provide the ratio between heat flow rate per voltage output - which represents the calibration coefficient, ε, of a calorimeter

$$\varepsilon = K/E \tag{2.9}$$

2.3.2 Calorimeter calibration

The heat flow sensors record the heat dissipated from the Li-Ion in terms of the voltage response. However, to measure the heat dissipated in units of watts, a calibration coefficient is required [13]. The calibration coefficient ε, is a constant that indicates the proportion between the calorimeter output (in voltage) and the thermal power input. A common method of determining the calibration heat conduction calorimeters is by electrical calibration [23]. This involves using a calibration heater (resistor) which is heated by passing a current I (A), and the corresponding voltage response is measured. The thermal power P (W) that is produced in the calibration heater with resistance R (Ω) can be obtained from

$$P = I^2R \tag{2.10}$$

There are two main types of electrical calibrations. The first type will keep the current on until steady state is reached i.e., steady-state calibration, and the second type being shorter thermal pulses, i.e., pulse calibration. The steady-state calibration is expressed as the aforementioned ε (P / U). While the pulse calibration represented as

$$\varepsilon = \frac{P\Delta t}{\int U dt} \tag{2.11}$$

where Δt (s) represents the duration of the pulse. Author Wadsö [23] reported that the calibration coefficient results for both methods differed by 0.12%, hence indicating they achieve similar results. Hence, in the following thesis work the steady-state calibration method is employed due to the simplicity and no need to consider thermal delay in measurement with each pulse.

An important aspect of conducting calorimetry experiments is in using a reference sample. The central idea being the reference (or second 'sample') should not produce any heat, but should have similar thermal properties as the sample. By using the reference, one can record the heat flow measurements of both the sample and the reference, where the difference between the two can be measured. If the calorimeter setup up reaches thermal equilibrium, then low noise and low drift will be measured. Author Wadsö [23] notes that the important property of the reference is that the thermal properties (e.g. heat capacity) should be similar, and that not the reference should not produce any heat. Considering calibration at different thermal powers, the general principle is that one should expect the voltage output from the heat flow sensors to follow a proportional relationship to the thermal power at steady state [23]. Therefore, the calibration coefficient should be independent to the thermal power level.

3
Case Setup

The following section aims to describe the methodologies followed during the calorimeter, cell assembly, cell characterisation and heat generation experiments. The main requirement of the experimental methodology is to address the objectives outlined in Section 1.2.1.

3.1 Overall Setup

The overall experimental setup is shown in Figure 3.1. The setup consists of a custom-build calorimeter that is housed in a styrofoam box. The working principle of the calorimeter was described in Section 2.3. The calorimeter consists of two sides labelled side A and side B, where in between the sample and reference cells are placed. Between the sample and reference, the styrofoam material is placed as to insulate the sample and reference from potential heat transfer.

The two sides of the calorimeter aluminium plates are integrated with the thermal heat sensors. On each side, there are two pairs of thermal sensors connected in series, giving a total of 8 - four on each side. The heat sinks on both side A and B have the water circulation flowing through and is controlled by the Julabo temperature regulator. To provide good contact, both plates are tightened using spring holders. The voltage output from the heat flow sensors on sides A and B for both sample and reference are added together - thus giving the total heat output from the sample. The voltage output in the thermal sensors are recorded using both the GAMRY tester and PICO logger. PT100 temperature sensors are used to measure the temperature on each side A and B of the calorimeter, the calorimeter indoor box temperature and the outside temperature. In total, 8 channels were used for recording the PT100 temperature using the PICO logger. The calorimeter was placed inside a large styrofoam box as to replicate a adiabatic environment where minimal heat is to escape to the outside environment. Finally, the isothermal bath system used was a Julabo F25MA which provided a constant supply of water at constant temperature.

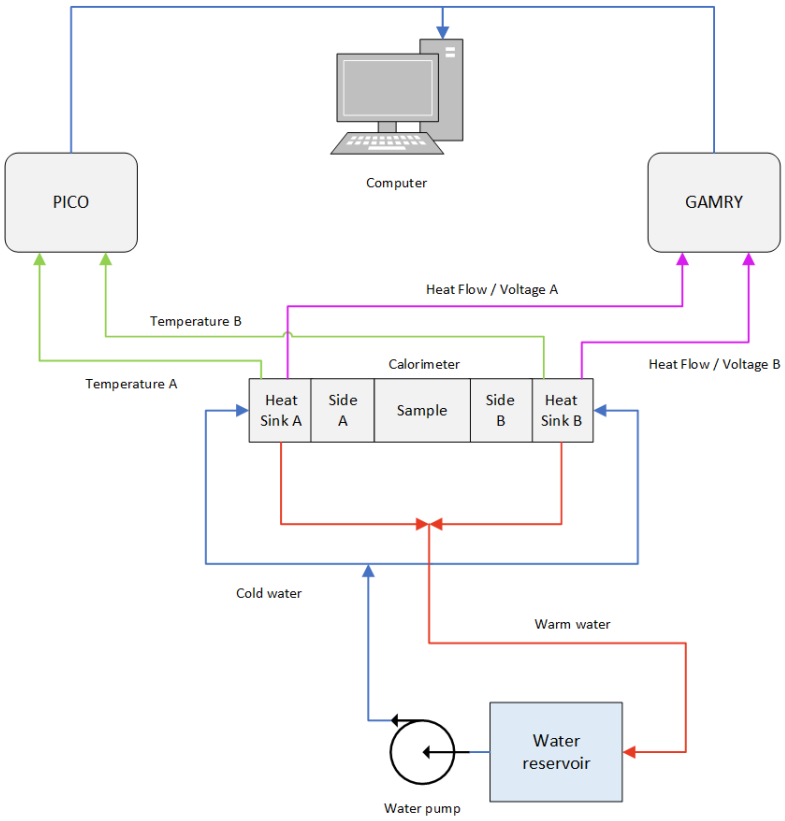

Figure 3.1: Overview of experimental setup. (Adapted from authors Lidbeck & Syed [13]).

3.2 Measuring equipment

The various measurement instruments used throughout the experimental work include the following:

- **GAMRY Reference 3000 potentiostat**: The battery tester is used to perform electrochemical tests on LIB cells such as charging and discharging cycles. The heat flow measurements (in mV), cell voltage output (V), and current (A) are measured using the GAMRY.

- **PT-104 Data Logger**: Temperature and heat flow measurement recorder in degrees celsius and milliVolt respectively.

- **FLUKE 787**: Multimeter used to measure voltage and resistance of sample in Volts and ohms respectively.

Table 3.1: Technical specifications of measurement equipment [13]

GAMRY 3000 Reference	
Operation limits	±15 V; 3.0 A or ±30 V; 1.5A
Potential applied accuracy	±1 mV ±0.2% of setting
Potential measured accuracy	±1 mV ±0.2% of reading
Current applied / measured accuracy	±5 pA ±0.05% of range
PT-104 Data Logger	
Compatibility	Works with PT100 and PT1000 sensors
Accuracy (unit of 23 ± 2 ∘C)	0.015 ∘C + 0.01% of reading
Resolution	0.001 ∘C

3.2.1 Calorimeter setup

The calorimeter device used during the experimentation is shown in Figure 3.2 a and consists of the following key features:

- **Heat flow sensor**: European Thermodynamics Peltier Module (GM200-31-14-10) rated at 1.08 W, 1.29 A, 1.7 V, 20x20 mm [1].

- **Twin calorimeter configuration**: Where the difference in heat output between the sample (side A) and the reference (side B) is registered.

- **Heat sinks**: Aluminium heat sink with to allow for heat to flow from heat source (sample cell) through the heat flow sensors and towards the heat sink.

- **Styrofoam box**: Box used to insulate the calorimeter from the external environment and thus replicating an adiabatic environment.

- **Temperature regulator**: Jalabo temperature regulator is used to achieve a temperature controlled environment where water circulates into the calorimeter at a desired temperature.

- **Copper sheets**: Copper sheets with high thermal conductivity is attached to the heat flow sensors as to increase heat transfer

- **Thermal pads**: Similar to the copper sheets, the thermal pads with high thermal conductivity is attached to both the heat flow sensors and copper sheets to increase heat transfer

3.2.2 Calibration heaters

To determine the calibration coefficient, a calibration heater as seen in Figure 3.2 b rated at 1.25 W and 12 V was used to determine the calibration coefficient [2]. Thermal pads were attached on both sides of the heater before placing the heater mats inside of aluminium foil bags as to replicate a pouch cell as seen in Figure 3.2 c. Author's Lidbeck & Syed [13] used two silicon rubber heater mats each rated at 15 W. The reason why a lower powered heater is because one of the key objectives of the thesis is to understand the sensitivity of the setup (by measuring low thermal heat flows).

Four wires were soldered onto the heater terminals (two on each terminal) as to create a four wire measurement configuration. During the calibration the heater mats are connected to the GAMRY instrument via the auxiliary channels, however the auxiliary channel can only measure voltage differences of ± 5V. Therefore, a voltage divider circuit was constructed in order to map the 12 V heater onto the GAMRY's auxiliary channel. The resistors selected in the construction of the voltage divider circuit were resistor 1 (R1) and 2 (R2) were 33 kΩ and 56 kΩ respectively. The sensing cable connected to one of the GAMRY's auxiliary channels would measure the voltage across the heater mat. With the voltage divider circuit implemented, the maximum voltage of heater mat was reduced to 4.45 V according to

$$V_{aux} = V_{rated}\frac{R1}{R1 + R2} = 12[v]\frac{33[k\Omega]}{33[k\Omega] + 56[k\Omega]} = 4.45[V] \tag{3.1}$$

where V_{aux} is the heater voltage inputted into the GAMRY auxiliary channels, V_{rated} is the rated voltage of the heater mat, R1 and R2 the resistor values.

3.2.3 Validating calibration coefficient

In addition Lidbeck & Syed performed calibration measurements at three different power levels for both sides of the calorimeter. The purpose of this was to investigate whether the calibration coefficient is consistent for varying power outputs of the calibration heater. A similar methodology was employed to validate the accuracy

(a) Top view of calorimeter inside styrofoam box

(b) Resistor heater mat

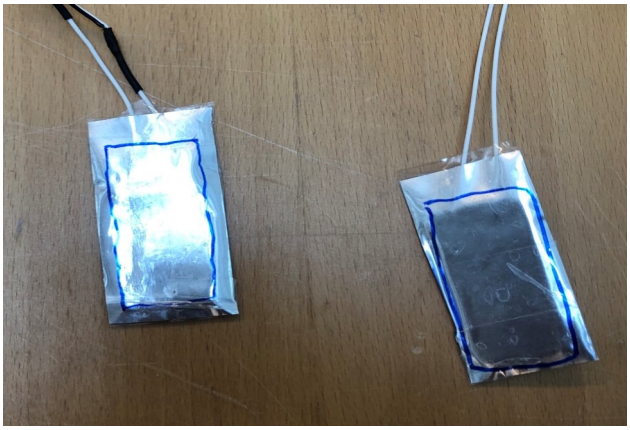

(c) Resistor heater mat in foil

Figure 3.2: Calorimeter and calibration setup

of the calibration coefficient determined. However, in addition to this, a second calibration experiment was performed to determine how low heat measurements could reliably be determined - hence, the second experiment aimed to gradually reduce the heat output until no heat measured could be determined.

3.3 Test Sample

The electrochemical and heat generation experiments were performed on lab-scale cells and a commercial cell. The following section aims to describe the assembly process of the lab-scale cell as well as the specifications of both the lab-scale cell and the commercial cell.

3.3.1 Lab-scale Cell Assembly Process

The lab-scale cells were assembled at Ångström Laboratory at Uppsala University where the following materials were used

1. **Cathode**: Single-coated lithium iron phosphate (LFP) with aluminium current collector; with circular geometry with 13 mm diameter.

2. **Anode**: Single-coated Graphite (with copper current collector) in circular shape with 13 mm diameter.

3. **Separator**: Separator of circular shape with 17mm diameter.

4. **Electrolyte**: Electrolyte composed of EC:DMC 1:1 1M LiPF 6 + 2% Vinilydene Carbonate (VC) and aluminum and copper tabs pre-cut

Firstly, aluminum foil sheets where used as pouch casing, and these were pre-cut into different sizes as shown in Figure 3.3 a and Figure b. The aluminum and copper tabs were then inserted in the pouches and sticky tape were used to keep the tabs stuck to the pouch casing. Thereafter, a heat sealer was then used to "weld" the pouch side that contains the tabs, sealed. The distance between the tabs were kept as close as possible (approx. 1mm), however not too far and conversely, not too close as to prevent short circuiting.

Soon after the potential difference was measured using a voltmeter, to perform a pre-check to ensure that the tabs are not in contact which would result in short-circuiting.r. The electrodes were dried over overnight (12 hours) at 120 degC using a pump vacuum in a glovebox to ensure that the electrodes contain minimal moisture content. Similarly, the separators were dried for 120 degC in the glovebox, however only during the day (5 hours).

Once the pouch cells were prepared, they were inserted inside a glovebox that contained inert atmospheric conditions due to argon gas being filled. The oxygen content in the glovebox was less than 1 ppm, and the relative humidity was 1.5 ppm. The electrodes were then weighed. After weighing, the assembly within glovebox began, where the separator was first inserted in the pouch between the two tabs, thereafter the respective electrodes were on the sides corresponding to the correct tabs (e.g. graphite facing separator and current collector facing copper, and LFP

facing separator and current collector facing aluminium). It was important that the separator completely covered both electrodes (hence larger diameter). It was equally important that each current collector was in contact with their corresponding tabs. Once the electrodes and separator were aligned, the electrolyte was inserted.

40-50 microliter of electrolyte as seen in Figure 3.3 c (in excess) was then inserted in the pouch between the separator and one of the electrodes. Once done, the pouch cells were then ready for vacuum sealing, where all sides of the pouch were sealed as shown in Figure 3.3 d. One side was sealed at 250 mBar. Once all cells, were assembled, the potential difference was again measured to ensure that no short-circuiting may have occurred as a result of errors during the assembly process.

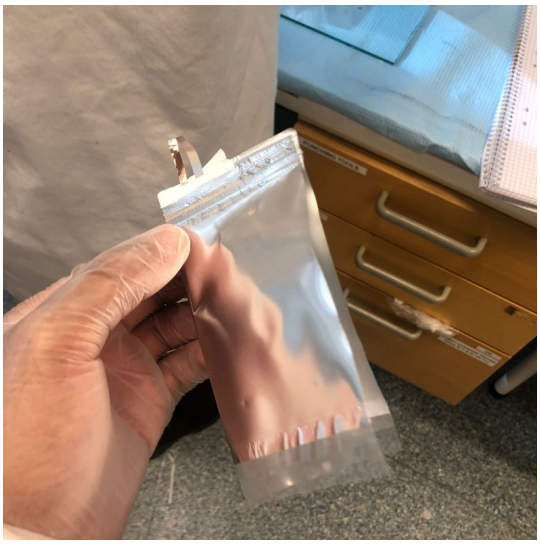

(a) Pouch cell before vacuum sealing

(b) Several full and half-cells

(c) Insertion of electrolyte into pouch

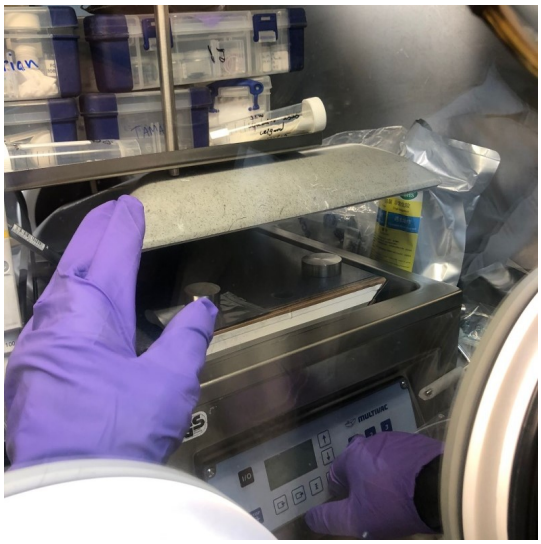

(d) Vacuum sealer for pouch cells

Figure 3.3: Cell assembly process at Uppsala University's Ångström Laboratory

3.3.2 Commercial cell

A commercial lithium-ion pouch cell as illustrated in Figure with the following specifications was also used during the experimental tests

Table 3.2: Properties for lab-scale full-cell

Capacity	850 mAh
Max charge voltage	4.2 V
Discharge cut-off voltage	3 V

3.4 Cell Characterisation

Characterisation of a LIB cell involves performing electrochemical tests that provide insight into the characteristics and performance qualities of a LIB cell.

3.4.1 Formation procedure

Before any pristine LIB cell can be cycled, a formation (or activation) procedure is required. The purpose of this is to develop a Solid Electrolyte Interphase (SEI) layer on the electrodes, especially on the anode. The formation cycle is ensures that the Li-ion is into the anode electrode and thus forming the SEI layer. This a critical component as the SEI layer provides a protective barrier between the electrolyte and the electrode. Therefore, a formation experiment was implemented on the pristine cells before the cells were cycled.

The formation cycle consisted of three full charge and discharge cycles at 0.1 current rate (C-rate) (265 micro A). For the LFP/Graphite full cell and the LFP/Li-ref half cell, the voltage was charged from OCV to 4.1 V and then discharged to 2.7 V. In between the charge/discharge cycles a rest period of 30 minutes was performed. For the Graphite/Li-ref, the formation procedure began with a discharge cycle, and then charge cycle, from 2 V to 0.05 V. These three charge/discharge cycles aimed to ensure the formation of the SEI layer on the graphite anode. A Biologic battery testers was used for the formation procedure at approximately 22.1 deg C.

3.4.2 EIS procedure

To gain insight into the resistance, or impedance of the lab-scale cells, an an Electrochemical Impedance Spectroscopy (EIS) test was performed on the cells.

The EIS procedure is a useful technique that can be used to characterize as well as quantify a LIB cell's internal resistance, charge transfer resistance, diffusion impedance, and double-layer capacitance which overall contribute to the impedance (resistance) of a LIB cell. The technique relies on perturbing, i.e., disturbing, an electrochemical system using alternating current (AC) signal instead of direct current (DC) signals. In the EIS procedure a small amplitude AC voltage or current is

applied to the LIB cell and this is referred to as perturbation. The frequency of the AC signal varies from kilohertz (kHz) to milliHertz (mHz) which allows for further analysis on the LIB cell over these frequencies. measured.

Typically EIS tests are performed in either Galvanostatic or Potentiostatic mode. Galvanostatic implies constant current is applied to the LIB cell while the potential may vary; while potentiostatic refers to constant potential (voltage) while the current may vary. Both modes were tested on the cells, and it was found that Galvanostatic mode gave more appropriate results. In order to model the impedance of the cells, the EIS results were fitted using the Z-view softeare, an equivalent circuit model was created where the internal resistance can be estimated from the fitted data. If a voltage perturbation is applied then the current is measured or vice versa. The measured response of the LIB cell can then be used to calculate the impedance of the system, where the impedance contains both a magnitude and a phase, and therefore it is a complex quantity. This impedance essentially is calculated as the ratio between the voltage perturbation to the current response or vice versa as well as the phase shift between the two. The two main methods for representing the impedance data is by way of a Nyquist plot or a Bode plote where the impedance is show over the frequency range.

3.5 Heat generation thermal parameters

Finally, in order tie together the aforementioned electrochemcial characterization tests, the following tests were performed to estimate the thermal parameters that contribute to the overall heat generation in the LIB cells.

3.5.1 Internal resistance (R_{int})

As seen in (2.7), the internal resistance (R_{int}) of a LIB cell is an important factor that governs heat generation in a lithium-ion. However, measuring the internal resistance has its challanges as a LIB cell is analogous to a non-linear and time dependant systems [22]. Hence, the approximation of a cells internal resistance is dependant on the method and experimental conditions which ultimately impact the outcome of measurements.

There are several techniques that can be used to determine the internal resistance of a LIB cell, namely the current pulse method, electrochemical impedance spectroscopy (EIS) and thermal loss methods [6]. The pulse method is a common technique used to determine the Ohmic resistance of a LIB cell. The method involves applying a current pulse (typically in Δ10 SOC intervals) and then the resulting voltage response in the cell is observed. The internal resistance, R_{int} can then be calculated by using Ohm's Law where V0, V1, and I represent the voltage before pulse, voltage after pulse and current respectively

$$R_{int} = \frac{V_1 - V_0}{I} \tag{3.2}$$

In evaluating R_{int}, the current pulse method (at every 20% SOC) and electrochemical impedance spectroscopy (EIS) were compared.

3.5.1.1 Open circuit voltage (E_{OCV})

The linear interpolation, Galvanostatic Intermittent Titration Technique (GITT) or simply, voltage relaxation methods, are effective ways for measuring the E_{OCV} [8][9]. The linear interpolation method consists of performing a complete charge and discharge cycle at low C-rates (ideally $I < C/10$). The idea is that at this low current rate the over-potential effect is minimized and consequently the instantaneous terminal voltage is estimated to be equal to the E_{OCV}. On the other hand the voltage relaxation method involves partially discharging the cell (at for example every 5% SOC interval) and then the voltage is measured after a rest period (commonly more than 2 hours). After each rest period (e.g., 2 hours), the potential is considered to be an approximation to E_{OCV}, as it is assumed that the cell's internal chemical reactions have reached a state of equilibrium (typically when the cell voltage variation is less than 0.1 mV in one minute) [9]. In this study, both methods were employed where fairly similar results were observed.

3.5.1.2 Entropic factor ($\frac{\partial E_{OCV}}{\partial T_{cell}}$)

The entropic factor or entropic coefficient, $\frac{\partial E_{OCV}}{\partial T_{cell}}$, can be obtained either through direct measurement, or by thermal loss calculations. The direct measurement consists of two methods: potentiometric and less commonly used calorimetric measurement [11]. The potentiometric method relies on measuring E_{OCV} of the LIB cell at different temperatures where E_{OCV} follows a linear relationship with the LIB cell temperature. The slope of the linear relationship is equivalent to the entropic coefficient, $\frac{\partial E_{OCV}}{\partial T_{cell}}$. In order to achieve accurate results it is recommended to use a high precision voltage measurement device that records once equilibrium has been reached. Although the potentiometric method gives decent accuracy, the method is time consuming due to the long relaxation and thermal equilibrium time required especially with larger sized LIB cells [11].

The less commonly used, calorimetric method involves measuring a LIB cell's entropic factor inside a calorimeter at constant temperature ideally at a low C-rate ($I \leq C/10$) as to minimize heating due to the over-potential, or the joule-heating effect. Since the calorimeter measures the total heat generated, one can subtract the heat caused by over-potentials (irreversible heating) from the average heat measured from the charging and discharging cycles, and thus arriving at the average entropy profile during charge and discharge (at the same C-rate).

The cell is is cycled at a 100% DoD (i.e., 0% to 100% SOC) in both charge and discharge directions. The advantage is one can avoid lengthy relaxation periods required at each SOC level, while still achieving a continues entropic coefficient profile. In this study the calorimetric method is used at 0.1 C and 22° C. Authors [11] performed similar experiments and reported that reliable results were obtained while performing this method.

While applying the calorimetic method, a crucial assumption is made, which is that the irreversible heat (due to ohmic resistance) is equal for both charge and discharge at the the same C-rate, and thus one can estimate the entropic coefficient by using the simplified Newman equation [22]

$$\frac{\partial E_{OCV}}{\partial T_{cell}} = \frac{Q_{discharge} + Q_{charge}}{2IT_{cell}} \tag{3.3}$$

where I, T, Q_{charge} and $Q_{discharge}$ respectively represent the current rate, cell temperature and heat losses during the charge and discharge cycles.

4

Calorimetry calibration results

As highlighted in 2.3.2, calibration experiments are a crucial component for the calorimetry experiments. The following section aims to provide the results of these experiments.

4.1 Calorimeter calibration

In the first calibration experiment, the heater was heated to the following power levels: 1.25 W, 1 W, 0.625 W, 0.25 W and 0.125 W. Where the corresponding voltage response at side A and side B sample and reference are illustrated in Figure 4.1b. It was observed that the voltage response from the thermal heat flow sensors was directly proportional to the thermal power supplied by the heater mats. This observation was also seen in the calibration coefficient, where it was observed to remain constant as the voltage output was proportional to the thermal power. Furthermore, it was observed that the heater mat produced more heat on one side hence in the measurement results side A produced a larger voltage signal compared to side B in the first experiment. The experimental setup was repeated two time and in both experiments the epsilon value remained relatively constant as seen in Figure 4.1b and Figure 4.1c.

Since the objective of the thesis work is to measure low thermal flows in the lithium-ion cells, a second round of calibration experiments were performed and this time the objective was to investigate the existing setups limitations in terms of sensitivity to heat flow measurement. During this calibration experiment, the heat power levels were the following: 0.625 W, 0.25 W, 0.125 W, 0.014 W and 6 mW. It was observed at lower power levels the noise readings increased, and thus impacting the calibration coefficient as reported by [23]. It was observed that the calibration coefficient was 0.0151 ± 0.019 V / W. At 6 mW, there was a clear distinction in the voltage signal for the sample S(A) and S(B) measurements (where the heater was placed) compared to the reference R(A) and R(B) as seen in Figure 4.2 a and b. At power levels lower than 6 mW, there was no clear distinction between the sample and reference and hence, 6 mW corresponding to the sensitivity limitations of the current setup.

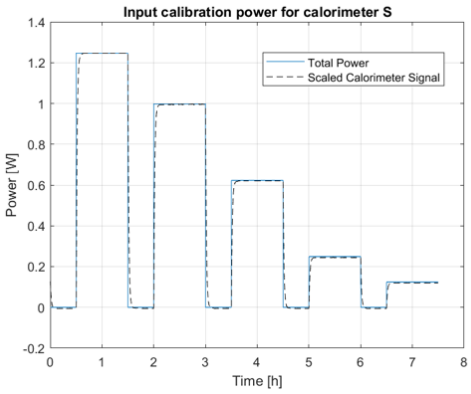

(a) Thermal output vs time

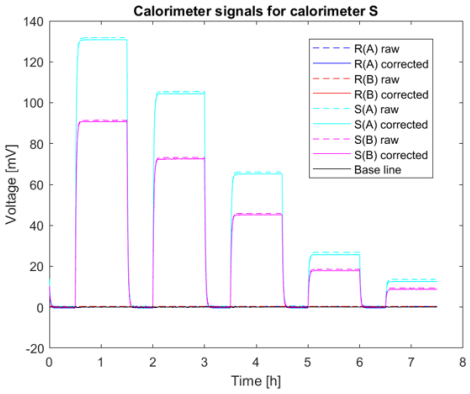

(b) Corresponding voltage output

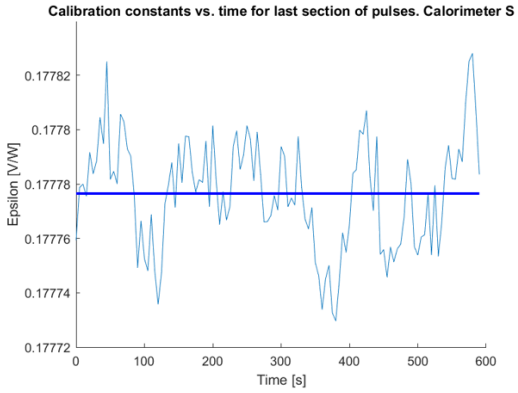

(c) Calibration Coefficient 1

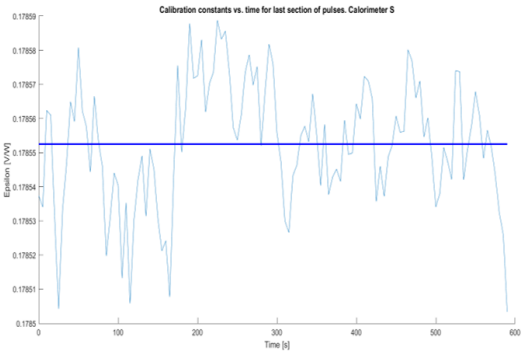

(d) Calibration Coefficient 2

Figure 4.1: Calorimetry calibration experimental results

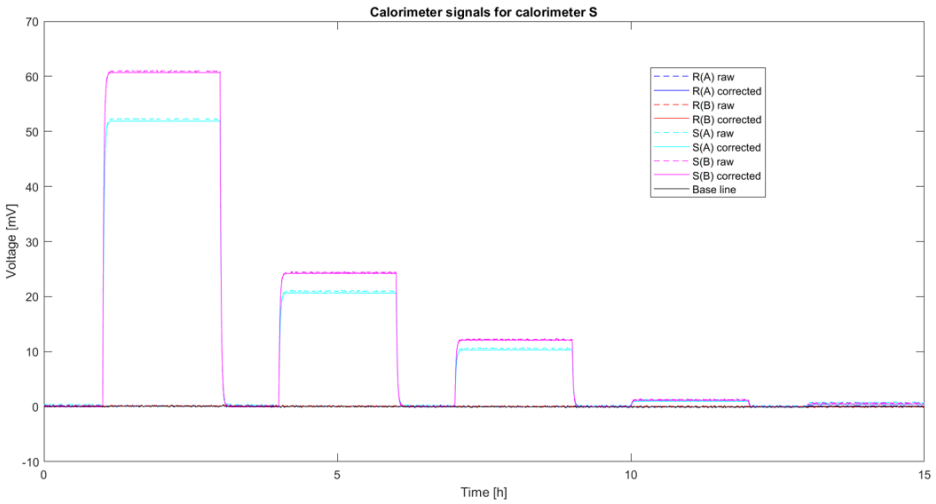

(a) Voltage output for 0.625, 0.25, 0.125, 0.014 and 0.006 W respectively

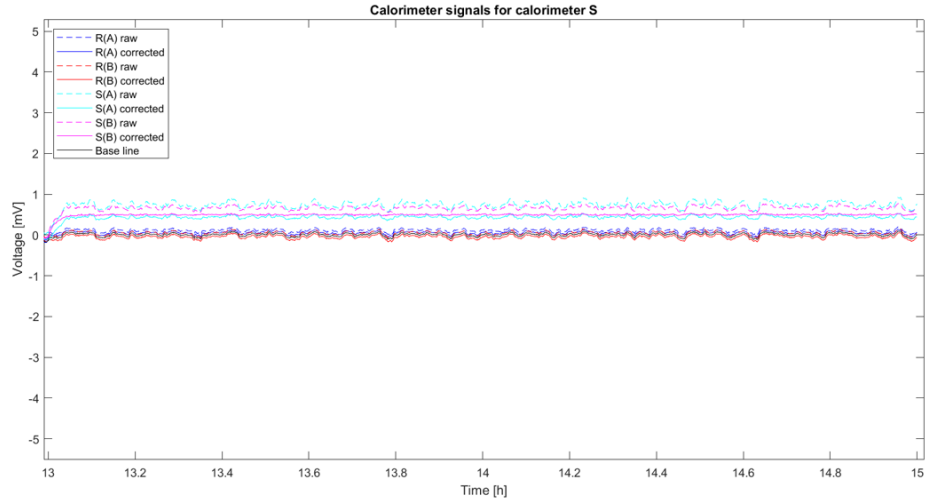

(b) Zoomed in voltage output for 6 mW power level

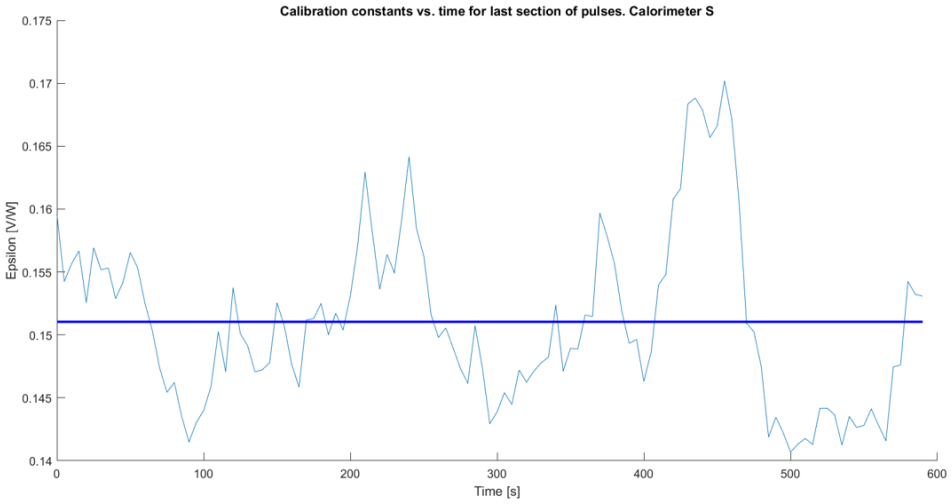

(c) Calibration coefficient at 6 mW

Figure 4.2: Calorimetry calibration experimental results

4.2 Cell characterization

As outlined in Section 3.3.1 the assemble of lab-scale cells was done, and the formation procedure discussed in Section 3.4.1 was performed.

Upon conducting the formation cycle, it was observed for the Graphite | LFP full cell, the voltage profile was in agreement to typical Graphite | LFP formation cycles. However, one can observe in Figure 4.3 b a voltage drop between the charge and discharge plateaus. This voltage drop is likely due to to the high impedance in the lab scale cells. This is typical in imperfect lab-scale cells, and results in lower quality performance compared to commercial cells.

As seen in Figure 4.3 c, the charge capacity is highest during the first cycle. During the initial cycle, the Li-ions transport from the positive electrode (LFP) through the electrolyte and intercalate into the negative electrode (Graphite), ultimately creating a stable solid-electrolyte interface (SEI) layer on the graphite surface. The SEI layer providing stability and protection of the Graphite surface layer, improving the cell's cycling stability. However, during the formation of the SEI layer, irreversible side reactions occur with the electrolyte, which further consume lithium ions and reduce the overall capacity of the cell. This phenomena is more pronounced in the charge capacity. Cycles 2 and 3 show a lower capacity, however the charge capacity begins to stabilize. The discharge capacity however, is shown to be stable across all three cycles during formation. The discharge capacity however, is lower than the theoretical capacity of 2.67 mAh as calculated in Appendix A.1.

In the LFP half-cell, the same formation procedure as the full cell was performed. Interestingly, the charge capacity was lowest in the first cycle, but increased to, and showed stability in cycle 2 and 3. There are possible reasons for this; there may have been incomplete activation of the cathode material resulting in a lower capacity in the first cycle. Furthermore, there may have been insufficient electrolyte penetration into the cathode further causing lower capacity. The discharge capacity remained relatively stable across all three cycles.

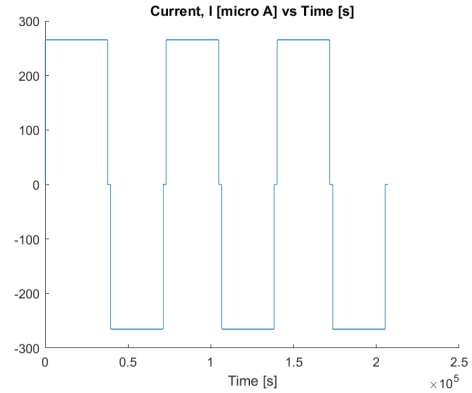

(a) Current vs Time

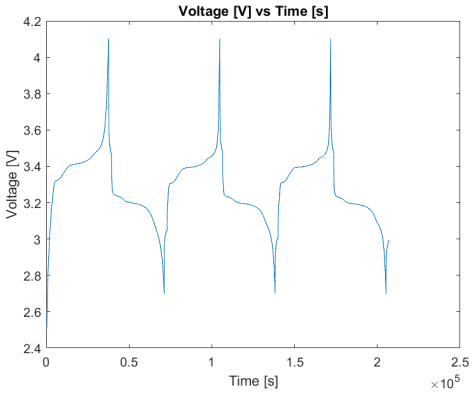

(b) Voltage profile

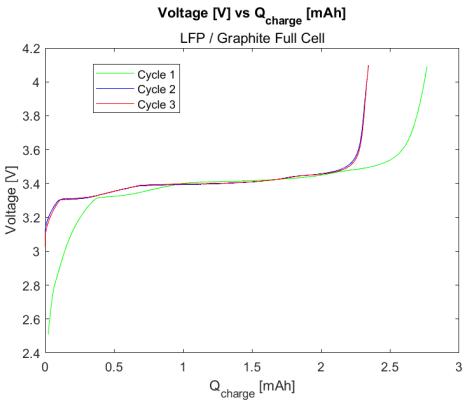

(c) Voltage vs Q_{charge}

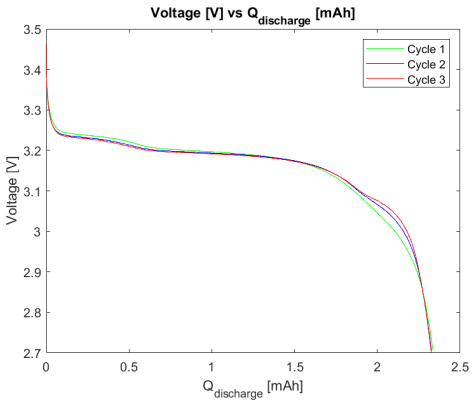

(d) Voltage vs $Q_{discharge}$

Figure 4.3: LFP/Graphite full-cell formation cycle results

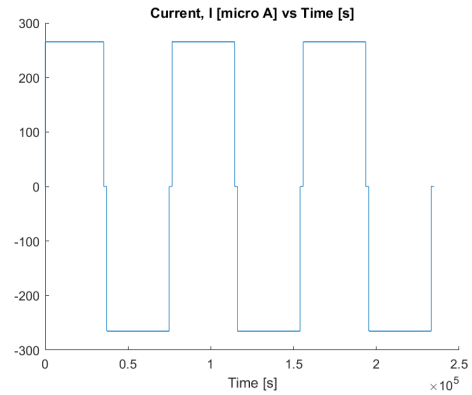

(a) Current vs Time

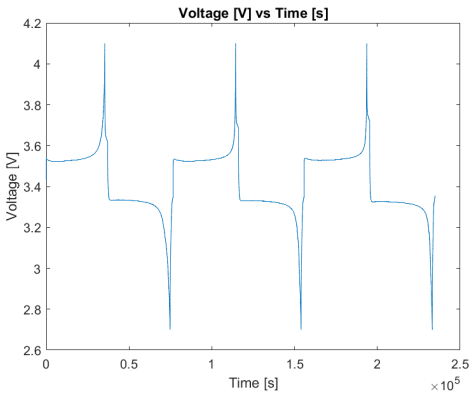

(b) Voltage profile

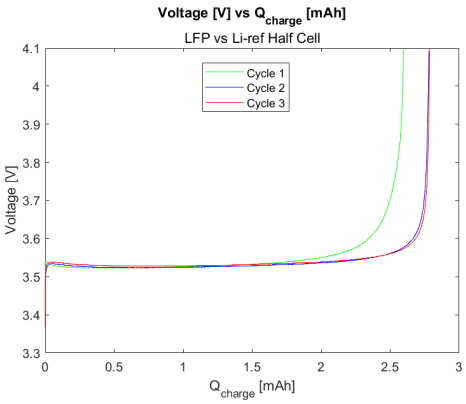

(c) Voltage vs Q_{charge}

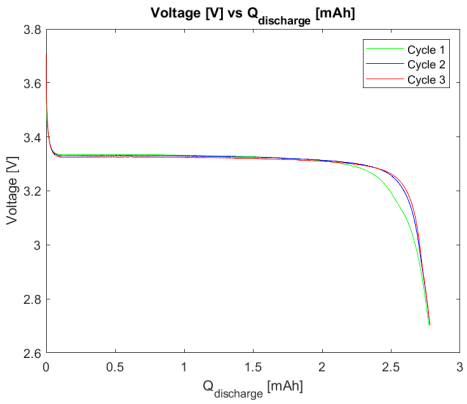

(d) Voltage vs $Q_{discharge}$

Figure 4.4: LFP half-cell formation cycle results

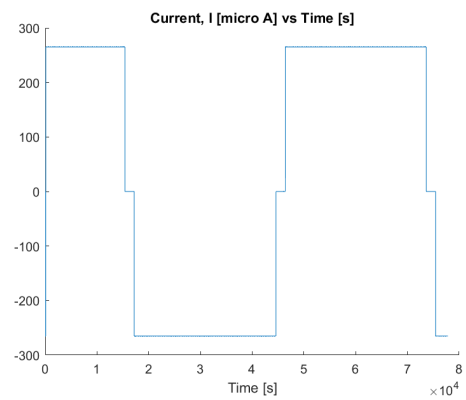

(a) Current vs Time

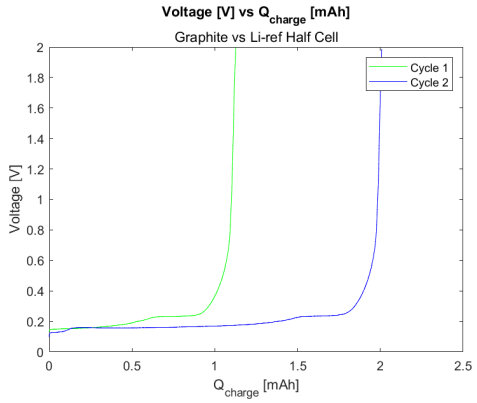

(b) Voltage profile

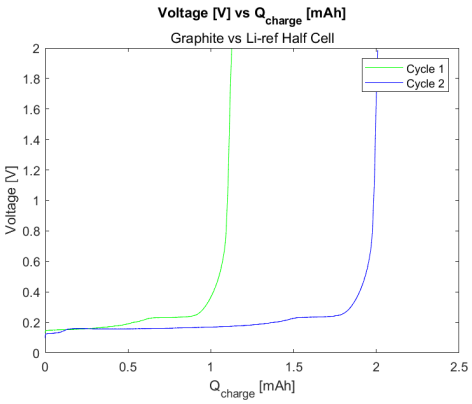

(c) Voltage vs Q_{charge}

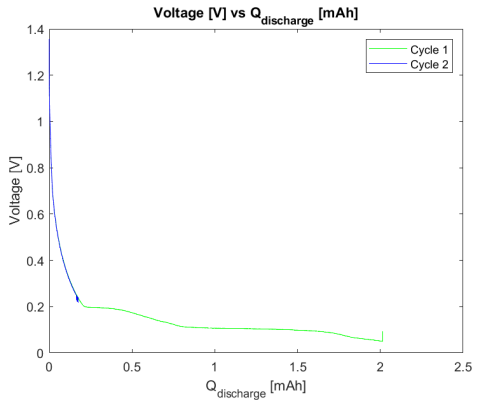

(d) Voltage vs $Q_{discharge}$

Figure 4.5: Graphite half-cell formation cycle results

4.3 Electrochemical characterization

4.3.1 Electrochemical impedance spectroscopy (EIS)

Upon completing the formation cycles, the actual charge and discharge capacities were determined and used for further electrochemical tests. An EIS test was performed at 50 % SOC as to estimate the cell's impedance. The EIS was performed in Galvanostatic mode between 100 kHz and 0.1 Hz. Figure 4.6 illustrates the impedance spectrum of the lab-scale cell, and a equivalent circuit model (ECM) fit created using ZView 4 a graphical analysis tool for EIS data. The ohmic (R0) and charge transfer resistance (R1) values of the cell were estimated to be 2 Ω and 220 Ω respectively as shown in Table 4.1. Compared to commercial LIB cells, unsurprisingly the resistance of the lab-scale cell was significantly high. The ECM also modelled the capacitance behaviour using the constant phase element (CPE) and the diffusion resistance (W01, Warburg impedance) using the Warburg element. Although not perfect, the ECM model gave a reasonable fit.

Table 4.1: Data values for ECM model of Graphite / LFP Full Cell

Element	Value
R0	2
R1	220
CPE1-T	3.87E-6
CPE1-P	0.872
Wo1-R	334
Wo1-T	3660
Wo1-P	0.38

4.4 Heat generation of lab-scale cells

Upon completing the characterisation tests on the lab-scale cells, heat generation experiments were performed in the calorimeter. A full depth-of-discharge (DoD) cycle was performed on the cells (0-100 % SOC) at 0.1 C (265 micro A) with 30 minutes of rest between each cycle.

The heat generation profile illustrated inconsistencies, for example during the first charge cycle the heat flow measurement pattern was moving in a downward direction (suggesting an endothermic behaviour) - while in the second charge cycle, the heat flow measurement pattern moved in an upward direction (suggesting an exothermic behaviour) as seen in Figure 4.7. To further investigate the inconsistencies, the sample heat measurements were compared to the reference measurements as seem in Figure 4.8. It was observed that the heat flow measurements for both sample and reference followed a similar pattern, strongly suggesting that the heat flow measurements in the sample area were not coming from the sample cell. To further investigate the source of this heat pattern, the calorimeter box temperature was compared, and indeed a similar but opposite temperature pattern was observed,

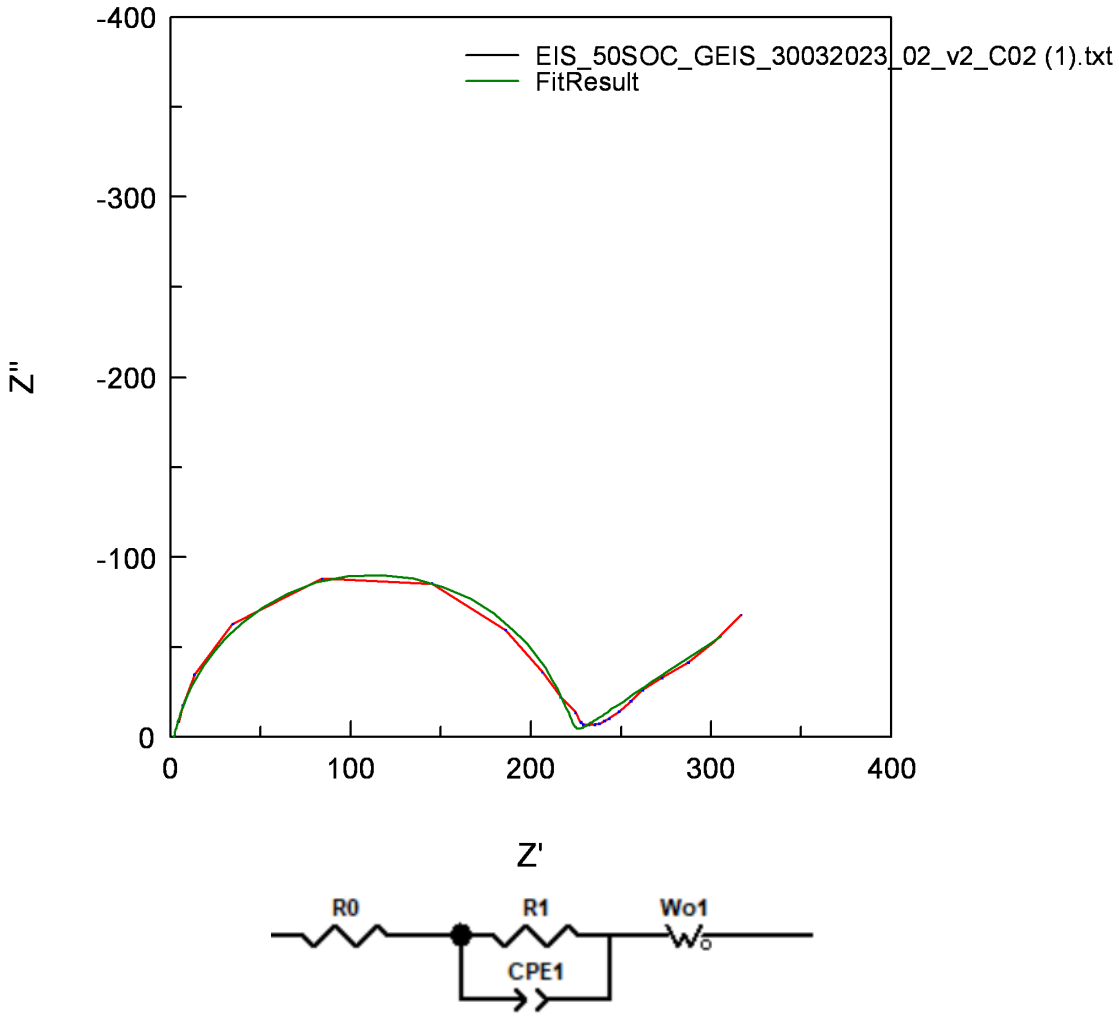

Figure 4.6: EIS and ECM model of Graphite / LFP full cell

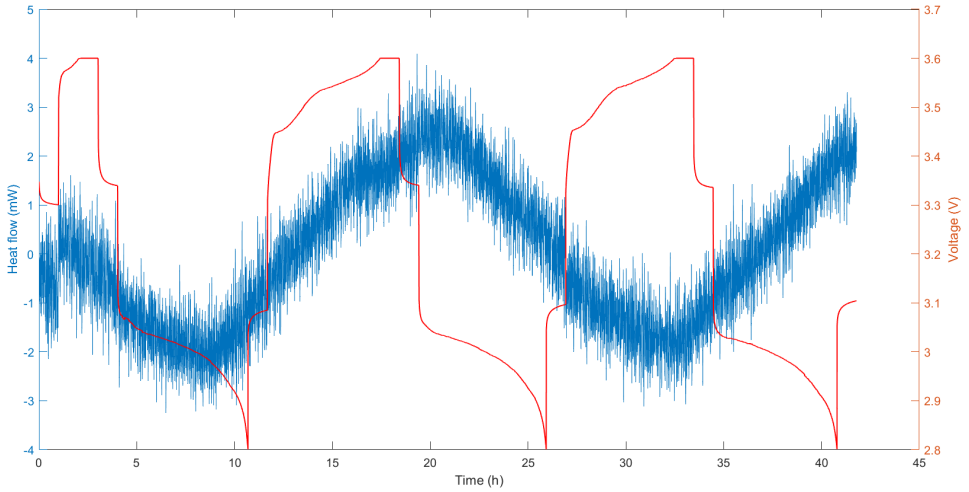

Figure 4.7: Heat generation and voltage profile of Graphite / LFP cell

indicating that the initial heat measurements were due to the fluctuating temperature of the calorimeter box. The most probable cause for this is heat leakage from inside of the calorimeter box to the outside environment. This is likely because the styrofoam box is not perfectly insulated an important learning for low thermal flow measurements.

By using (2.10), the applied current of 1 C and ohmic resistance value, R0 (as seen in Table 4.1) were used to estimate the expected heat generation of the cell. It was determined that the order of magnitude of the cell was in micro Watts. As seen in Section 4.1 the existing calorimeter setup is not sensitive enough to measure heat generation on the microWatt level.

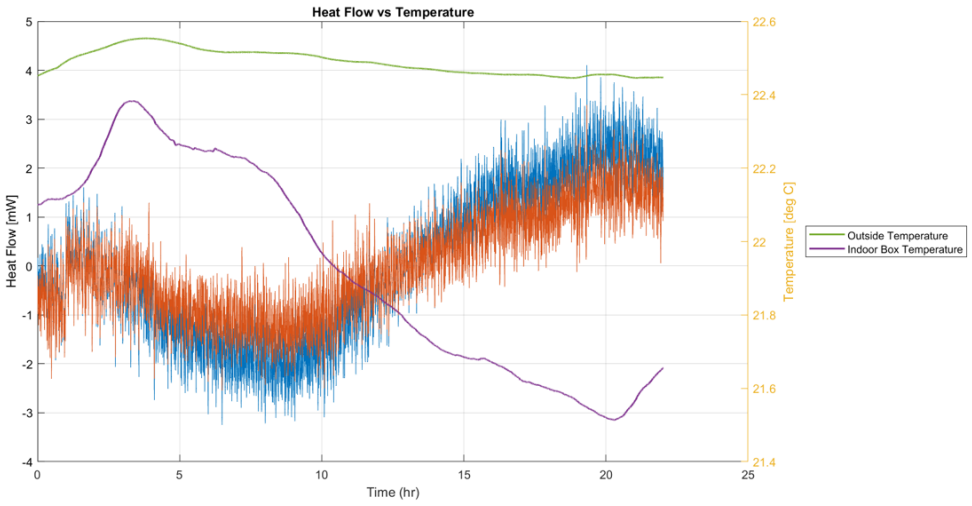

Figure 4.8: Heat flow readings of Sample and Reference side including temperature readings of the inside calorimeter box and outside ambient temperature.

5

Electro-thermal properties

During the measurement of heat generation, initially the heat generation rate of the lab-scale cells were measured. However, due to the low magnitude of heat dissipated/absorbed from the cells, the calorimeter setup was unable to produce reliable results. In addition to the high levels of noise in the readings, the challenge of shifting baseline was observed. Meaning, as the length of the experiment increases, the baseline heat measurement reading too shifts. Hence, with the current setup, the lab-scale cells could not be measured due to low heat generation from the cells. Hence, the 850 mAh commercial lithium-ion pouch cell outlined in Section 3.2 was instead used for heat generation experiments.

As seen in Section 3.5, the electro-thermal properties of a LIB cell underpin the electrical and thermal characteristics that impact a LIB cells performance and safety. The following section aims to present the results from the the aforementioned methods used to obtain these electro-thermal properties on the 850 mAh commercial pouch cell.

5.1 Internal Resistance, R_{int}

The internal resistance, R_{int} was determined using several methods, mainly pulse method and electrochemical impedance spectroscopy (EIS).

The first method that was used was the charge pulse method where the LIB cell was charged continuously at 0.1 C from 0-100% SOC, where at each Δ20% SOC increment the LIB cell was held at constant SOC and allowed to reach a stable open-circuit voltage by allowing 2 hours of rest. After the rest period, a 1 C charge pulse was applied for 10s before the voltage response of the LIB cell was measured, and where the resistance could be determined using Ohm's Law. Figure 5.1 illustrates the cell's internal resistance (R_{int}) after applying the current pulse method at 22 °C. It is evident that when applying a charge pulse, the internal resistance is at it's highest at 0% SOC thereafter decreasing and remaining relatively stable. A EIS test was also performed on the commercial cell at Δ 10% SOC in the charge direction. Similarly to the 1C Pulse test, it was observed that the charge transfer resistance was highest at 0 % SOC, while the ohmic resistance was constant. This could indicate that the reason for the high resistance in the pulse test due to the contributions of the charge transfer resistance.

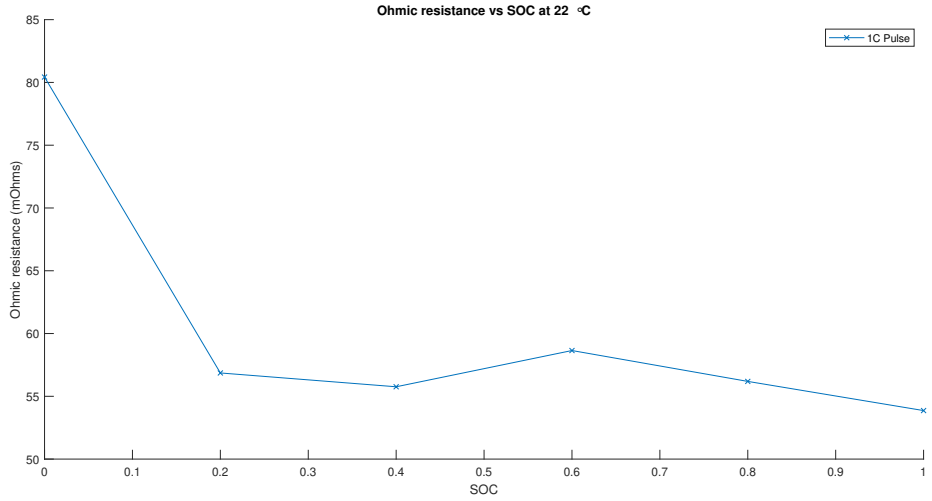

Figure 5.1: Pulse resistance test at 1C Pulse and 0.1 C charge

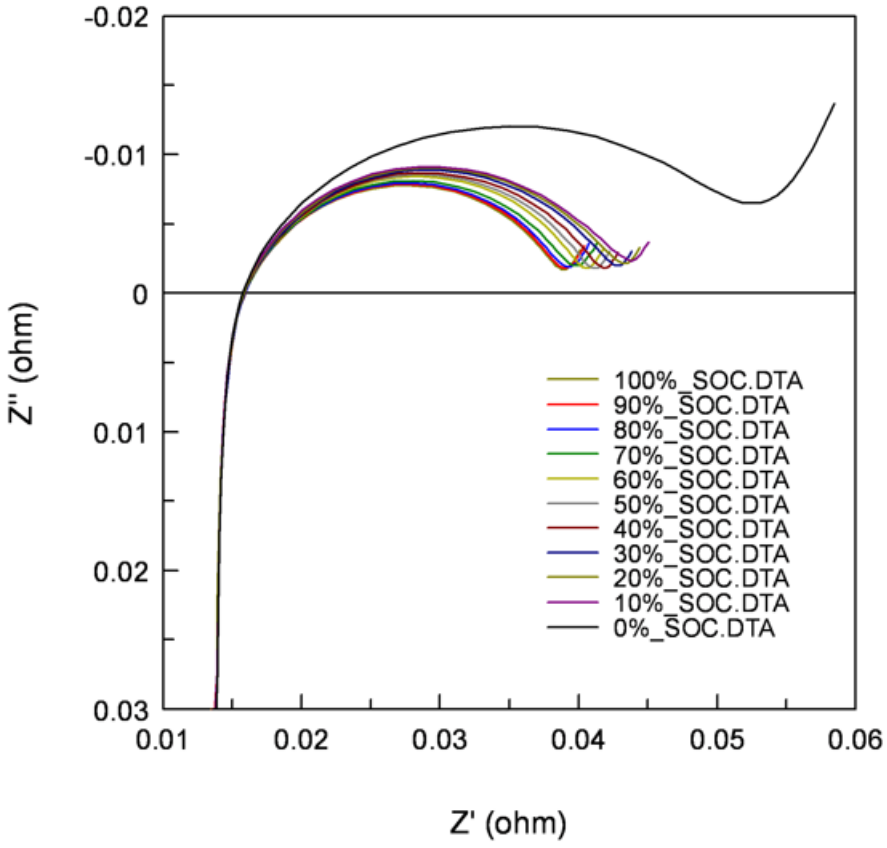

Figure 5.2: Hybrid EIS at every 10% SOC at 22 deg C

5.2 Open circuit voltage, E_{OCV}

To obtain the OCV-SOC curve displayed in Figure 5.3 of the 850 mAh LiPo pouch cell, the cell was cycled at a low current rate (C = 0.1) at 22 deg °C, thus reducing the over-potential affect allowing for the measured instantaneous voltage to be close to OCV. Despite the cell having an unknown chemistry, the OCV-SOC curve shown in Figure 5.3 fairly resembles the OCV-SOC curves for both LMO and NCA. Figure 5.3 shows good similarity to the OCV-SOC curved reported by [11], hence LMO and/or NCA based chemistries being highly plausible.

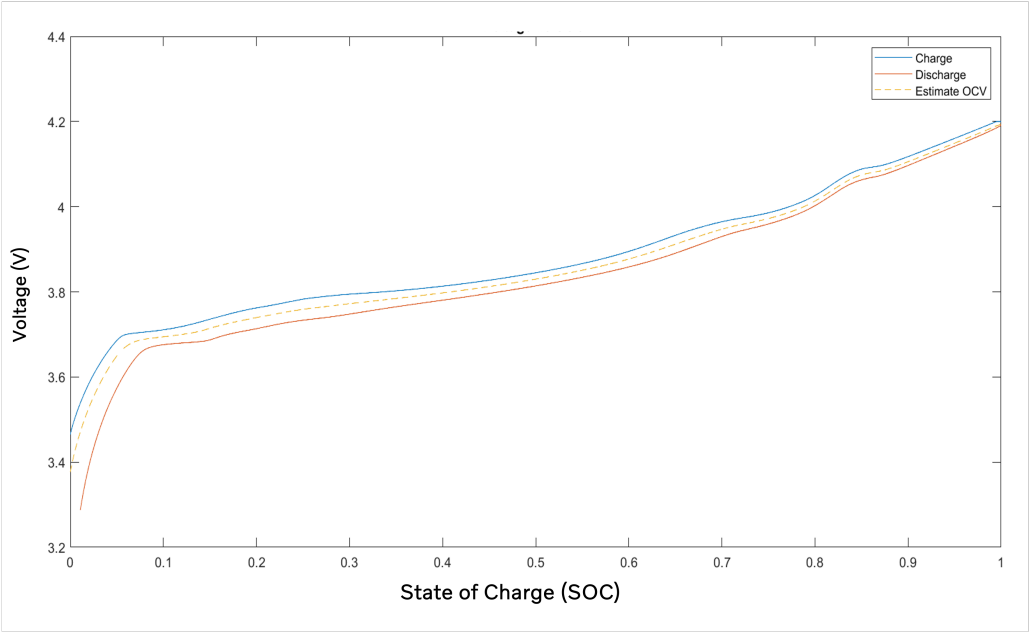

Figure 5.3: The estimated open circuit voltage curve (OCV)based on 0.1 C charge and discharge

The entropic factor ($\frac{\partial E_{OCV}}{\partial T_{cell}}$) was obtained using the calorimetric method. Since the calorimetric method measures the total heat generated, it is necessary to subtract the the irreversible heat generated in order to estimate the reversible heat, and therefore the entropic factor. To estimate the irreversible heat generated the battery cells over-potential (ohmic resistance) or R_{int} was used from the. The entropic factor via calorimetric measurement provides fairly accurate results and repeatable results, while being comparatively quick to produce. This allows for continuous entropic coefficient profiles to be achieved, which can made useful to thermal models. However, the calorimetrer equipment tend to be costly. The entropic factor from calorimetric measurement was also compared to the thermal loss calculation method as shown by Thomas et al. [19].

6
Heat Generation

In the following chapter, heat generation experiments were performed on the 850 mAh pouch cell under various C-rates, and ambient conditions. Furthermore, the contributions of the irreversible and reversible heat generation were separated using the calorimeter technique.

6.0.1 Effect of C-rate on heat generation

Upon cycling the cell under different C-rates one could observe immediately that the higher the C-rate the higher the heat flow measurement as illustrated in Figure 6.1. During the charge cycles, the commercial cell was cycled from 0 % to 100 % SOC with 0.1, 0.5, 1 and 2 C current rates. The maximum charge rate of the cell is 2 C. In the discharge direction, the cell was discharged from 100 % to 0 % SOC with 0.1, 0.5, 1, 2 and 3 C current rates. Considering the discharge cycle, it was clear that with an increase in current, the heat generation increases quadratically due to the domination of irreversible heat generation at higher current rates as seen in Figure 6.2 - the reason for this is as seen in the irreversible heat equation (2.6) the current is squared for the irreversible heat contribution, while for the reversible heat contribution it increases linearly with current.

It was further observed that during discharge it was mainly exothermic (positive heat values). On the other hand, in the charge direction, both endothermic and exothermic behaviour was observed. While charging, very strong endothermic behaviour was observed between 0-40 % SOC, while beyond 40 % exothermic behaviour was observed, especially at higher C-rates. This behaviour was also reported by [17] where a lithium-cobalt (LCO) cell was cycled; possibly indicating that the commercial test sample may be based on LCO chemistry in the cathode.

6.0.2 Reversible and irreversible heat generation

The entropic profile of the cell was obtained through the calorimetric method. First the total heat generated for both charge and discharge at 100% DoD was measured at 0.1 C and 22 deg C as shown in Figure 6.3. Since the cell was cycled at 0.1C heating due to the Joule effect (irreversible heat) can be minimized. One can observe that the heat generation profile for the LIB cell follows a mirrored pattern between the charge and discharge cycles. Authors Shao et al. [16] have cited that the intercalation/de-intercalation pathway of the Li ion is the same during both

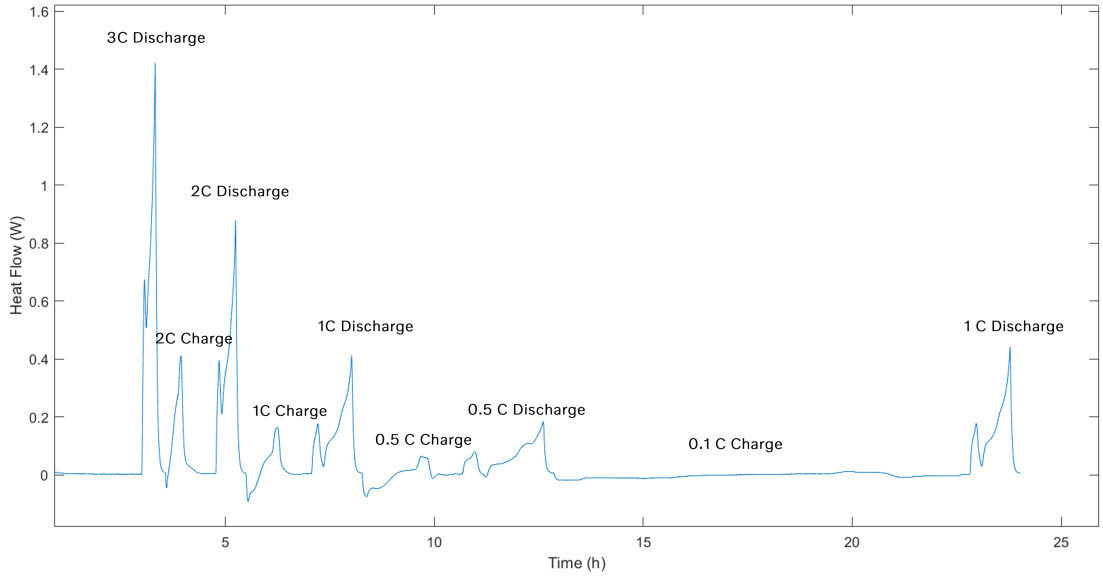

Figure 6.1: Heat flow over time for various C-rates

charge and discharge. Therefore, the transformation follows the same path, hence it is a reversible process and is symmetrical.

One can estimate the reversible profile by subtracting the irreversible heat contributions. To estimate the irreversible heat contribution, one can subtract the open circuit voltage from the cell's voltage output according to

$$Q_{irreversible} = I(E - E_{OCV}) \tag{6.1}$$

Figure 6.4 and Figure 6.5 illustrate the total heat generation including the estimated irreversible heat generation. It was observed that at 0 % SOC, the irreversible heat generation peaks and this could be due to the contribution of the charge transfer resistance peaking at 0 % SOC as seen in Section 5.1. Since the irreversible heat generation is estimated, one can now subtract this from the total heat generation measured in the calorimeter and ultimately estimate the reversible heat contribution. This was done for both charge and discharge processes, and the average of the two was further estimated. Authors [11] state that a possible reason why the entropic profile for charge and discharge are not identical could be due to over-potential or polarization contributions - which perhaps can be reduced if the open circuit voltage curve is estimated at a lower C-rate or after long relaxation times-

Figure 6.6, illustrates the entropic profile of the LIB cell where the entropic coefficient is plotted against SOC. One can observe that there is a very strong endothermic behaviour at low SOC conditions (negative entropic coefficient) dominating between 0-40% SOC (especially at 0%), while exothermic behaviour (positive entropic coefficient) dominating from 40 to around 80% SOC. Between 80 % to 100 % SOC negative entropic values are visible. Authors Velumani & Bandsal [21] reported that

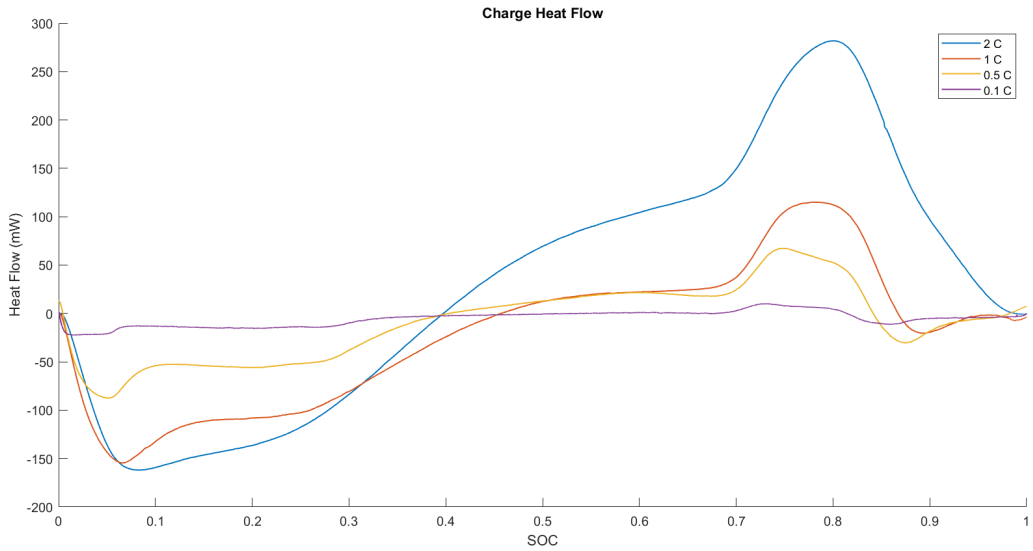

(a) C-rate vs SOC in charge direction

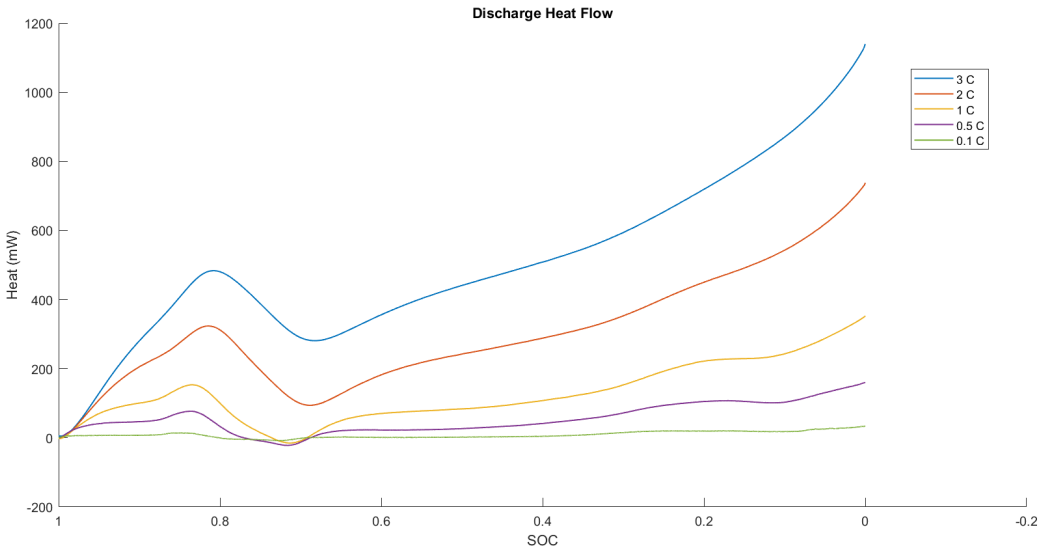

(b) C-rate vs SOC in discharge direction

Figure 6.2: Effect of C-rate on SOC

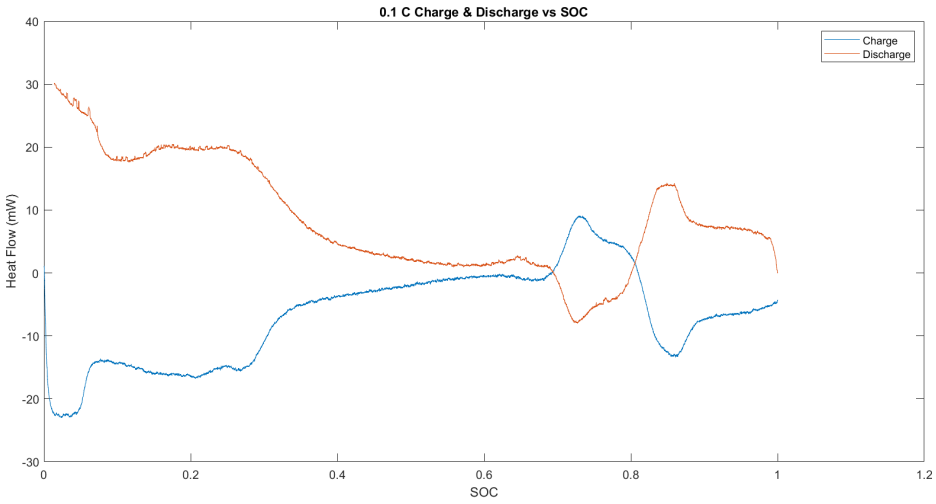

Figure 6.3: Heat flow [mW] vs SOC at 0.1 C for both charge and discharge at 22 deg C

a possible reason that the entropic values shift from negative to positive when cycling from 0% to 100% is due to crystalline phase changes during Li-ion intercalation. Authors Al Hallaj et al. [5] showed that the aforementioned entropic trend is due to crystallographic phase change of $LiCoO_2$ from hexagonal to monoclinic, before returning to hexagonal. They further highlighted that the order in which these Li-ions fill the sublattice is SOC dependant. This ultimately influences the reversible heat generated in the LIB cell, as heat absorption (endothermic) occurrs when the sublattice is empty, and heat release (exothermic) when the closest sublattice is full. The entropic profile illustrated in Figure 6.6 is in good agreement with authors [17] who have performed electrochemical experiments on LCO/graphite cells. They reported a distinctly negative entropic coefficient at low SOC and increasing between 60-70% SOC. Furthermore, they note that the entropic profile is in dependant on the cycling conditions (although slightly smaller at lower temperatures).

6.0.3 Effect of temperature

The effect of the cell temperature on heat generation was also investigated. This was achieved by varying the temperature of the Julabo temperature control. Before each electrochemical test was performed, a rest period was of 3 hours was applied, as to ensure that the inside temperature of the calorimeter box (and consequently the cell surface temperature) is at the desired temperature. Three temperature levels namely 10, 22 and 30 °C respectively, where 22 °C representing the base-case temperature. The temperature of the cell indeed has an impact on the overall heat generation as displayed in Figure 6.7 and 6.8. For both 1 and 2 C charge rates, the heat generated at 10 °C was highest, whereas the instantaneous heat generated was lowest at 30 °C. This is likely due to the overall contribution of the irreversible heat generated that dominate at C-rates greater than 1. This observation has been

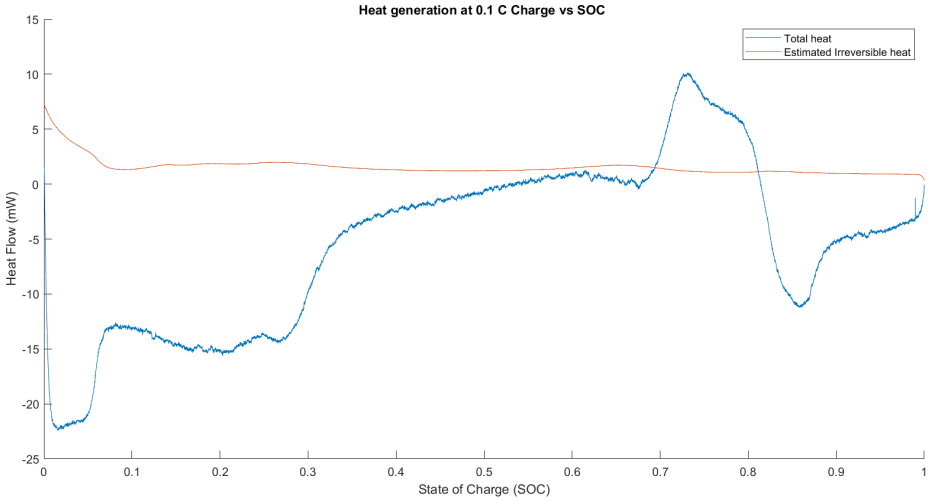

Figure 6.4: Charge total heat vs estimated irreversible

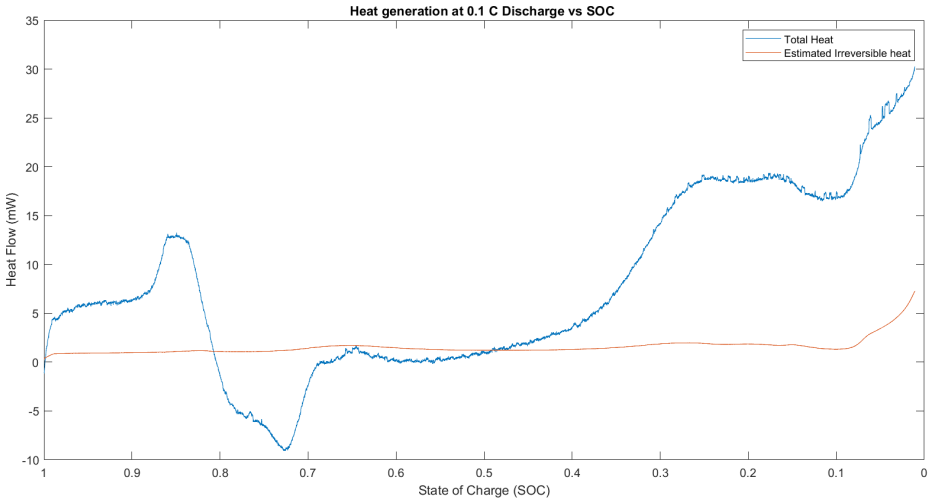

Figure 6.5: Discharge total heat generated vs estimated irreversible

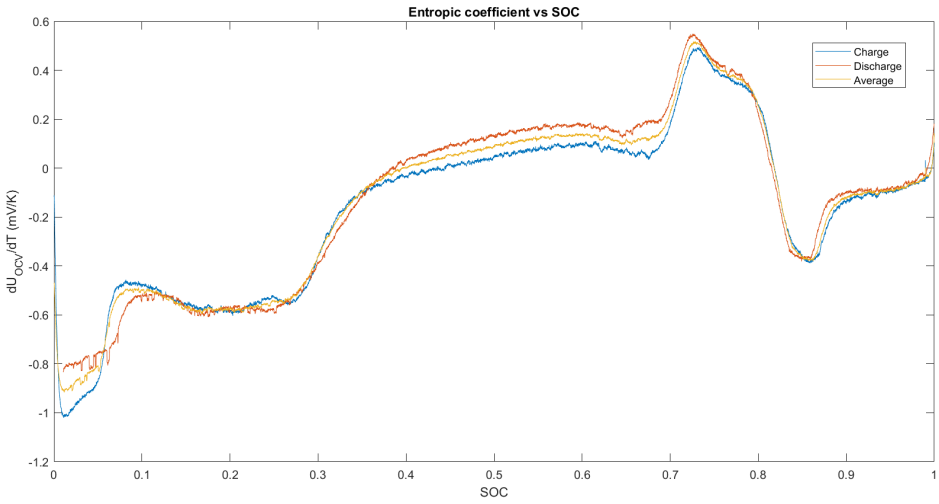

Figure 6.6: Entropic profile

reported, and is ultimately due to the increase in resistance and polarization in at lower temperatures, and vice-versa at higher temperatures.
Conversely, the impact of the cell temperature on overall heat generation was not significant at 0.1 C. This is due to reversible heat generation effects largely at play. Instead, the impact of the ambient temperature is linear on the entropic profile

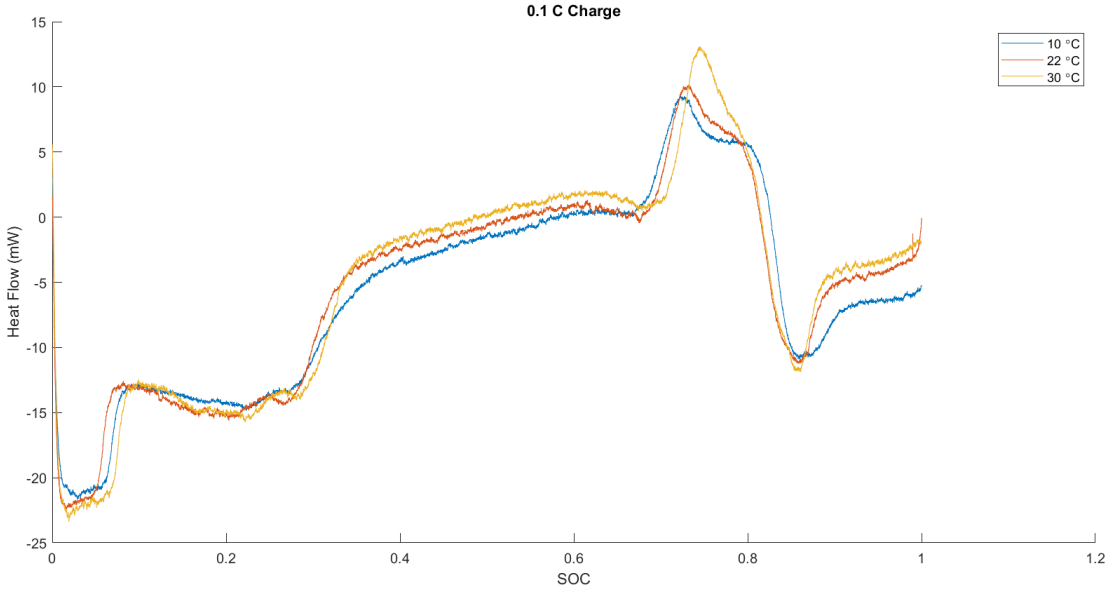

Figure 6.9: Cumulative at different C-Rates

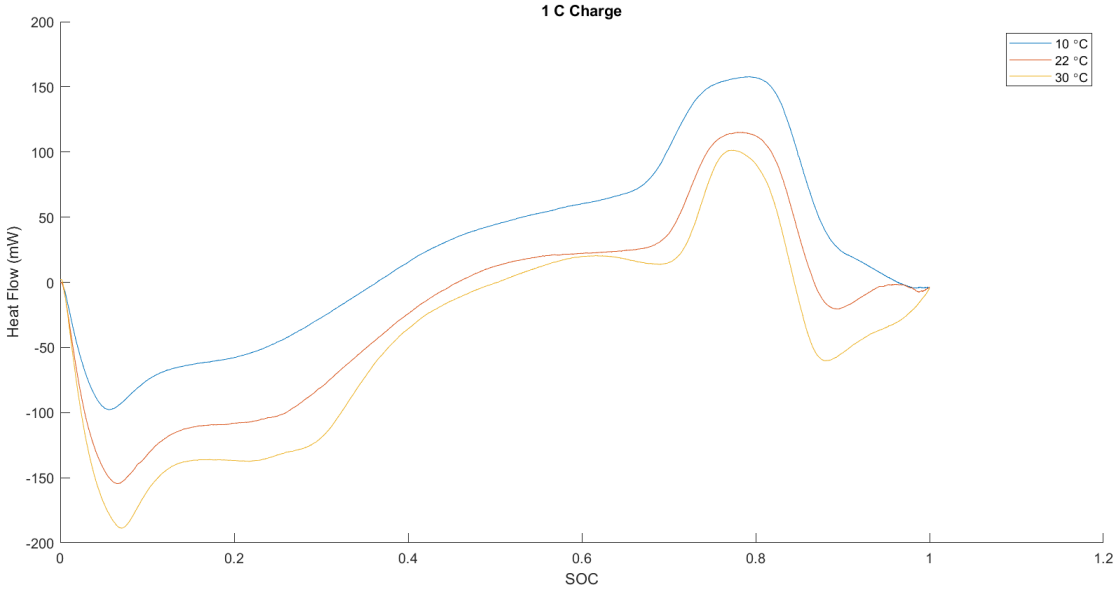

Figure 6.7: Cumulative at different C-Rates

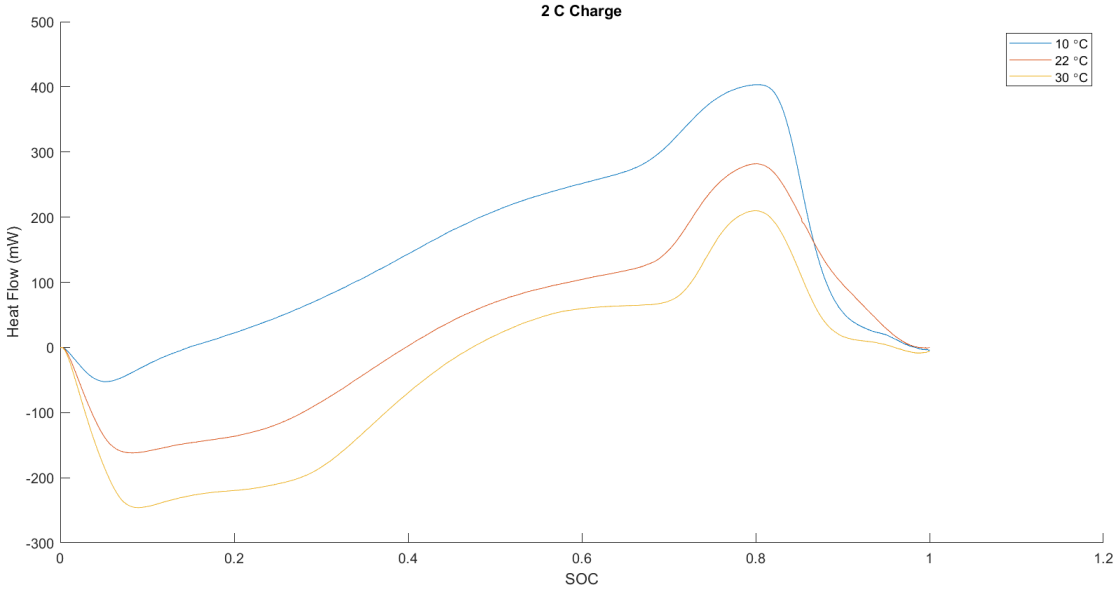

Figure 6.8: Cumulative at different C-Rates

7
Conclusion

The sensitivity of the calorimeter setup was improved and the limitations of the calorimeter sensitivity was found to be as low as 6 mW. The lab-scale cells assembled showed reasonable electrochemical performance after characterization methods were employed, however due to the low capacity and thus low current rates applied to the cells, the heat generated was not detectable in the existing calorimeter setup. One main source for high noise in the heat generation experiments on the lab-scale cell is heat leakage in the calorimeter box due to imperfect insulation and changing temperature in the outside environment. Hence, heat generation experiments were not successful on the lab-scale cells, and instead focus was shifted towards experiments on a 850 mAh commercial pouch cell. The heat generated from the commercial cell was sufficient enough for the calorimeter setup, and the total heat as well as the separation of irreversible and reversible heat generations were estimated by using the calorimetric technique.

Heat generation is a complex phenomena and is influenced by various factors such as degradation mechanisms, ageing, internal resistance and environmental conditions. The SOC window interval is another key parameter that influences the magnitude of heat generation where 0-20% and 80-100% SOC intervals, the heat generation is as it's highest. One possible reason for this, is that the internal resistance is highest at these SOC extremes, notably 0 % for the commercial cell. Another parameter that has seen an influence in the heat generation of the LIB cell is ambient temperature (i.e. cell surface temperature), where at higher temperatures LIB cell heat generation is lower due to lower internal resistance. The total generated is also largely dependant on the cell design as heat generation is pronounced in imbalanced cells (i.e. excess of anode material). More generally, heat generation is significant in aged cells (higher number of cycles and therefore lower SOH) due to increase in resistance and polarization effects in the cells. Finally, it was observed that the reversible heat generation of the cell dominates at lower C-rates, and the cell exhibits both endothermic and exothermic behaviour in the charge direction depending on the SOC level.

7.1 Future Work

In order to validate the quality and conclusions made in the thesis work, there are several aspects that can be improved. The following recommendations are:

- An important improvement to the existing calorimeter setup would be to improve the insulation of the calorimeter box. As highlighted in the conclusion chapter, it was noticed that heat leakage was a primary factor for poor sensitivity of heat generated from the lab-scale cells. In addition, the existing box set-up was prone to disturbances due to it being located at the entrance of the lab . Therefore, it is recommended that the set-up be isolated as much as possible from any undesired disturbances.

- Since the challenge of poor insulation and isolation of the calorimeter set-up (which resulted in limited sensitivity), it is recommended that lab-scale cells of higher capacity be assembled to increase the amount of heat generated. Lab-scale cells of 30 mAh and larger are recommended to achieve the 6 mW sensitivity limitation of the calorimeter set-up. Multi-layered electrodes design is a potential approach to achieving cells of higher capacity.

- Another interesting aspect that can be studied, is the effect of different cell chemistries on the heat generation trends observed. For example, LIB cells with NMC and NCA could be compared.

- Finally, a physics based simulation of the sample cells heat generation will provide valuable information to help validate the results observed in the thesis. For example, COMSOL could be used to both model the lab-scale cells and the commercial cells studied, which then can be compared providing greater certainty on the validity of the results achieved.

Bibliography

[1] European thermodynamics peltier module, gm200-31-14-10. https://se.rs-online.com/web/p/peltier-modules/7650003, Accessed 2023-06-11.

[2] Rs pro silicon heater mats. https://se.rs-online.com/web/p/heater-pads/0245499, Accessed 2023-01-25.

[3] Transport. 2022. https://www.iea.org/topics/transport, Accessed 2023-06-08.

[4] Ieee code of ethics. 2023. https://www.ieee.org/about/corporate/governance/p7-8.html, Accessed= 2023-06-08.

[5] S Al Hallaj, R Venkatachalapathy, J Prakash, and JR Selman. Entropy changes due to structural transformation in the graphite anode and phase change of the licoo2 cathode. *Journal of the Electrochemical Society*, 147(7):2432, 2000.

[6] Todd M Bandhauer, Srinivas Garimella, and Thomas F Fuller. A critical review of thermal issues in lithium-ion batteries. *Journal of the Electrochemical Society*, 158(3):R1, 2011.

[7] Helena Berg. *Batteries for electric vehicles: materials and electrochemistry*. Cambridge university press, 2015.

[8] D Doerffel. Testing and characterization of large lithium-ion batteries for electric and hybrid vehicles. *School of engineering sciences: University of southhamptom*, 2007.

[9] Christophe Forgez, Dinh Vinh Do, Guy Friedrich, Mathieu Morcrette, and Charles Delacourt. Thermal modeling of a cylindrical lifepo4/graphite lithium-ion battery. *Journal of Power Sources*, 195(9):2961–2968, 2010.

[10] Simone Franzò and Alessio Nasca. The environmental impact of electric vehicles: A novel life cycle-based evaluation framework and its applications to multi-country scenarios. *Journal of Cleaner Production*, 315:128005, 2021.

[11] Zeyang Geng, Jens Groot, and Torbjörn Thiringer. A time-and cost-effective method for entropic coefficient determination of a large commercial battery cell. *IEEE Transactions on Transportation Electrification*, 6(1):257–266, 2020.

[12] Thomas Hofelich, Lars Wadsö, Allan L Smith, Hamid Shirazi, and S Rose Mulligan. The isothermal heat conduction calorimeter: a versatile instrument

for studying processes in physics, chemistry, and biology. *Journal of Chemical Education*, 78(8):1080, 2001.

[13] Anton Lidbeck and Kazim Syed. Experimental characterization of li-ion battery cells for thermal management in heavy duty hybrid applications. Master's thesis, 2017.

[14] David Linden. Handbook of batteries. In *Fuel and energy abstracts*, volume 4, page 265, 1995.

[15] Bharathy S. Parimalam and Brett L. Lucht. Reduction reactions of electrolyte salts for lithium ion batteries: Lipf6, libf4, lidfob, libob, and litfsi. *Journal of The Electrochemical Society*, 165(2):A251, jan 2018.

[16] Weiwei Shao, Beibei Zhao, Wenjuan Zhang, Yan Feng, Wenfeng Mao, Guo Ai, and Kehua Dai. Study on the reversible and irreversible heat generation of the lithium-ion battery with lifepo4 cathode. *Fire Technology*, 59(2):289–303, 2023.

[17] Lena Spitthoff, Markus Solberg Wahl, Jacob Joseph Lamb, Paul Robert Shearing, Preben JS Vie, and Odne Stokke Burheim. On the relations between lithium-ion battery reaction entropy, surface temperatures and degradation. *Batteries*, 9(5):249, 2023.

[18] Peiyi Sun, Roeland Bisschop, Huichang Niu, and Xinyan Huang. A review of battery fires in electric vehicles. *Fire technology*, 56:1361–1410, 2020.

[19] Karen E Thomas, Christian Bogatu, and John Newman. Measurement of the entropy of reaction as a function of state of charge in doped and undoped lithium manganese oxide. *Journal of the Electrochemical Society*, 148(6):A570, 2001.

[20] Ozan Toprakci, Hatice AK Toprakci, Liwen Ji, and Xiangwu Zhang. Fabrication and electrochemical characteristics of lifepo4 powders for lithium-ion batteries. *KONA Powder and Particle Journal*, 28:50–73, 2010.

[21] Deepika Velumani and Ankit Bansal. Thermal behavior of lithium-and sodium-ion batteries: A review on heat generation, battery degradation, thermal runway–perspective and future directions. *Energy & Fuels*, 36(23):14000–14029, 2022.

[22] G Vertiz, M Oyarbide, H Macicior, O Miguel, I Cantero, P Fernandez De Arroiabe, and I Ulacia. Thermal characterization of large size lithium-ion pouch cell based on 1d electro-thermal model. *Journal of Power Sources*, 272:476–484, 2014.

[23] Lars Wadsö. Operational issues in isothermal calorimetry. *Cement and Concrete Research*, 40(7):1129–1137, 2010.

[24] Songrui Wang. Entropy and heat generation of lithium cells/batteries. *Chinese Physics B*, 25(1):010509, 2015.

A

Appendix 1

A.1 Theoretical capacity calculations for lab-cell

$Diameter_{electrode}$ = 13 mm
$Diameter_{separator}$ = 17 mm
$Area_{electrode} = \pi r^2 = \pi(6.5)^2 = 1.33 cm^2$

LFP active material = 2.01 mAh per cm^2
Capacity LFP = 2.01 [mAh per cm^2] * 1.33 [cm^2]= 2.67 mAh
Specific capacity graphite = 300 mAh per gram
Graphite active material = 7.5 mg per cm^2 = 9.9795 * 10^{-3} g
Capacity Graphite = 2.9925 mAh

N/P ratio = 2.9925 mAh / 2.67 mAh = 1.12

DEPARTMENT OF SOME SUBJECT OR TECHNOLOGY
CHALMERS UNIVERSITY OF TECHNOLOGY
Gothenburg, Sweden
www.chalmers.se

CHALMERS
UNIVERSITY OF TECHNOLOGY